

---

# Variational Autoencoding Discrete Diffusion with Enhanced Dimensional Correlations Modeling

---

**Tianyu Xie<sup>1,\*</sup>, Shuchen Xue<sup>3</sup>, Zijin Feng<sup>4</sup>, Tianyang Hu<sup>5</sup>,  
Jiacheng Sun<sup>4</sup>, Zhenguo Li<sup>4</sup>, Cheng Zhang<sup>1,2,†</sup>**

<sup>1</sup> School of Mathematical Sciences, Peking University

<sup>2</sup> Center for Statistical Science, Peking University

<sup>3</sup> Academy of Mathematics and Systems Science, Chinese Academy of Sciences

<sup>4</sup> Huawei Noah’s Ark Lab

<sup>5</sup> National University of Singapore

## Abstract

Discrete diffusion models have recently shown great promise for modeling complex discrete data, with masked diffusion models (MDMs) offering a compelling trade-off between quality and generation speed. MDMs denoise by progressively unmasking multiple dimensions from an all-masked input, but their performance can degrade when using few denoising steps due to limited modeling of inter-dimensional dependencies. In this paper, we propose Variational Autoencoding Discrete Diffusion (VADD), a novel framework that enhances discrete diffusion with latent variable modeling to implicitly capture correlations among dimensions. By introducing an auxiliary recognition model, VADD enables stable training via variational lower bounds maximization and amortized inference over the training set. Our approach retains the efficiency of traditional MDMs while significantly improving sample quality, especially when the number of denoising steps is small. Empirical results on 2D toy data, pixel-level image generation, and text generation demonstrate that VADD consistently outperforms MDM baselines.

## 1 Introduction

Diffusion models (Ho et al., 2020; Song et al., 2020) have shown their remarkable successes in generative modeling of continuous objects, e.g., image (Rombach et al., 2021; Ramesh et al., 2022), audio (Kong et al., 2021; Liu et al., 2023), and video (Ho et al., 2022; Blattmann et al., 2023). Recently, diffusion models have also been extended to the discrete state space (Austin et al., 2021; Campbell et al., 2022; Sun et al., 2023; Lou et al., 2024), achieving competitive or even superior performance to autoregressive models in tasks such as Sudoku solving and code generation. A notable example is the masked diffusion model (MDM) (Sahoo et al., 2024; Shi et al., 2024; Ou et al., 2025), which works by progressively masking the dimensions of the data point towards an all-masked state in the forward process, and gradually unmasking (i.e., predicting the distributions of) multiple dimensions simultaneously in the backward process. This parallel prediction capability allows MDMs to generate samples much faster than autoregressive models, which typically predict one dimension at a time.

Despite the inference efficiency of MDMs, their denoising distribution at each backward step is typically modeled as a product of independent categorical distributions across dimensions which may fail to capture complex inter-dimensional dependencies commonly present in real-world data. This

---

<sup>\*</sup>This work was done during an internship at Huawei Noah’s Ark Lab. Email: [tianyuxie@pku.edu.cn](mailto:tianyuxie@pku.edu.cn)

<sup>†</sup>Corresponding author. Email: [chengzhang@math.pku.edu.cn](mailto:chengzhang@math.pku.edu.cn)

issue becomes particularly pronounced when using a small number of denoising steps, where many dimensions must be unmasked simultaneously, amplifying the impact of independence assumptions. While recent efforts (Xu et al., 2024; Liu et al., 2024) have attempted to mitigate this limitation, they require inner-loop sampling steps under guidance from pre-trained autoregressive models or correlation models, introducing additional computation costs.

In this work, we propose Variational Autoencoding Discrete Diffusion (VADD), a novel framework that enhances discrete diffusion models by incorporating a latent variable structure into the denoising distribution. This structure enables the model to implicitly capture inter-dimensional correlations, thereby improving its approximation capacity. To address the intractability of the resulting marginal distributions, we adopt the variational autoencoding framework (Kingma & Welling, 2014), jointly optimizing the denoising model and an auxiliary recognition model via a variational lower bound. Beyond standard latent-variable sampling, we introduce a consistency sampler that fixes the latent variable throughout the entire backward process, empirically leading to higher-quality samples. We further design a specialized transformer-based architecture for VADD that retains the fast inference efficiency of traditional MDMs. Through experiments on 2D toy datasets, pixel-level image generation, and text generation, we show that VADD consistently outperforms MDM baselines—particularly in terms of sample quality—highlighting the benefits of modeling dimensional dependencies.

## 2 Background

**Masked diffusion models** Let  $\mathbf{x}_0$  be a categorical sample with  $N$  dimensions and  $\mathbf{x}_0^i \in \{1, \dots, V\}$  be the  $i$ -th dimension of  $\mathbf{x}_0$ . We further augment the state space with a special mask state  $[\text{M}] = V+1$ . Let  $\delta_a$  denote a one-hot vector of length  $V+1$  with the value 1 at position  $a$ . The forward process of masked diffusion models (MDMs) is defined as  $q(\mathbf{x}_t | \mathbf{x}_s) = \prod_{i=1}^N q(\mathbf{x}_t^i | \mathbf{x}_s^i)$  and  $q(\mathbf{x}_t^i | \mathbf{x}_s^i) = \text{Cat}(\mathbf{x}_t^i; \frac{\alpha_t}{\alpha_s} \delta_{\mathbf{x}_s^i} + \frac{\alpha_s - \alpha_t}{\alpha_s} \delta_{[\text{M}]})$  for  $s < t$ , where the mask schedule  $\alpha_t$  is a strictly decreasing function in  $t \in [0, 1]$  with  $\alpha_0 \approx 1$  and  $\alpha_1 \approx 0$ . Particularly, we have  $q(\mathbf{x}_t^i | \mathbf{x}_0^i) = \text{Cat}(\mathbf{x}_t^i; \alpha_t \delta_{\mathbf{x}_s^i} + (1 - \alpha_t) \delta_{[\text{M}]})$  that will diffuse to an all-masked state  $[\text{M}]^N$  at  $t = 1$ .

Given  $\mathbf{x}_0$ , the posterior distribution of  $\mathbf{x}_s$  takes the form  $q(\mathbf{x}_s | \mathbf{x}_t, \mathbf{x}_0) = \prod_{i=1}^N q(\mathbf{x}_s^i | \mathbf{x}_t^i, \mathbf{x}_0^i)$  where

$$q(\mathbf{x}_s^i | \mathbf{x}_t^i, \mathbf{x}_0^i) = \begin{cases} \text{Cat}(\mathbf{x}_s^i; \delta_{\mathbf{x}_t^i}), & \mathbf{x}_t^i \neq [\text{M}], \\ \text{Cat}(\mathbf{x}_s^i; \frac{1 - \alpha_s}{1 - \alpha_t} \delta_{[\text{M}]} + \frac{\alpha_s - \alpha_t}{1 - \alpha_t} \delta_{\mathbf{x}_0^i}), & \mathbf{x}_t^i = [\text{M}]. \end{cases} \quad (1)$$

Equation (1) inspires parametrizing the backward transitions as

$$p_{\theta}(\mathbf{x}_s | \mathbf{x}_t) = q(\mathbf{x}_s | \mathbf{x}_t, \mathbf{x}_0 = \mu_{\theta}(\mathbf{x}_t, t)) = \prod_{i=1}^N q(\mathbf{x}_s^i | \mathbf{x}_t^i, \mathbf{x}_0^i = \mu_{\theta}^i(\mathbf{x}_t, t)), \quad (2)$$

where the denoising distribution  $\mu_{\theta}(\mathbf{x}_t, t) \in \mathbb{R}^{N \times (V+1)}$  with the constraint  $\sum_{j=1}^V \mu_{\theta}^{i,j}(\mathbf{x}_t, t) = 1$  and  $\mu_{\theta}^{i,[\text{M}]}(\mathbf{x}_t, t) = 0$  is expected to match the posterior of the clean data  $q(\mathbf{x}_0 | \mathbf{x}_t)$ . The  $\mu_{\theta}(\mathbf{x}_t, t)$  is explicit and often trained by maximizing the continuous-time evidence lower bound (ELBO) (Shi et al., 2024; Sahoo et al., 2024)

$$\mathcal{L}(\mathbf{x}_0; \theta) = \int_0^1 \mathbb{E}_{q(\mathbf{x}_t | \mathbf{x}_0)} \frac{-\alpha_t'}{1 - \alpha_t} \log p_{\theta}(\mathbf{x}_0 | \mathbf{x}_t) dt \leq \log p_{\theta}(\mathbf{x}_0) \quad (3)$$

for all  $\mathbf{x}_0$  in the training set, closely related to any-order autoregressive models (Ou et al., 2025).

Note that the backward transition  $p_{\theta}(\mathbf{x}_s | \mathbf{x}_t)$  in equation (2) is factorizable over  $N$  dimensions which helps reducing the modeling complexity of state space. However, this conditional independence structure fails to capture the inter-dimensional correlations and would inevitably introduce cumulative approximation errors. As the number of dimensions unmasked simultaneously during a backward transition is proportional to  $(\alpha_s - \alpha_t)$ , this drawback can be more severe under a large step size.

**Variational autoencoders** Consider the generative modeling task on a dataset  $\{\mathbf{y}_1, \dots, \mathbf{y}_M\}$ , where  $\mathbf{y}_i$  is an  $N$ -dimensional continuous or discrete variable. The variational autoencoder (VAE) (Kingma & Welling, 2014) assumes a generative model  $p_{\theta}(\mathbf{y}, \mathbf{z}) = p_{\theta}(\mathbf{y} | \mathbf{z})p(\mathbf{z})$ , where  $\mathbf{z} \in \mathbb{R}^d$  is a latent variable with a prior distribution  $p(\mathbf{z})$ , and a recognition model  $r_{\phi}(\mathbf{z} | \mathbf{y})$  as an approximation

for the intractable posterior  $p_{\theta}(z|y)$ . The generative model and recognition model can be jointly learned by maximizing the following evidence lower bound (ELBO)

$$L(y; \theta, \phi) = \mathbb{E}_{r_{\phi}(z|y)} \log \left( \frac{p_{\theta}(y, z)}{r_{\phi}(z|y)} \right) = \log p_{\theta}(y) - D_{\text{KL}}(r_{\phi}(z|y) \| p_{\theta}(z|y)) \leq \log p_{\theta}(y) \quad (4)$$

for all data points  $\{y_1, \dots, y_M\}$ . Here,  $p_{\theta}(y) = \int_{\mathbb{R}^d} p_{\theta}(y, z) dz$  is the marginal likelihood of  $y$  and  $D_{\text{KL}}$  is the Kullback-Leibler (KL) divergence.

A mean-field structure is often assumed for the conditional distribution  $p_{\theta}(y|z)$ , i.e., the dimensions of  $y$  are independently distributed conditioned on  $z$ . As a comprehensible example, Kingma & Welling (2014) assumes the following distribution over a continuous image sample  $y$

$$p_{\theta}(y|z) = \mathcal{N}(\mathbf{m}_{\theta}(z), \text{diag}\{\sigma_{\theta}^2(z)\}), \quad (5)$$

where  $\mathbf{m}_{\theta}, \sigma_{\theta} : \mathbb{R}^d \rightarrow \mathbb{R}^N$  are two learnable neural networks. As a latent variable model, the marginal distribution  $p_{\theta}(y)$  is still capable of modeling the complex dimensional correlations by integrating out the latent variable  $z$ .

### 3 Methodology

In this section, we propose Variational Autoencoding Discrete Diffusion (VADD), which extends the dimension-independent denoising distribution in MDMs by introducing a latent variable structure. This design enables VADD to capture complex dependencies across dimensions. Both the denoising distribution and an auxiliary recognition model are jointly optimized under the variational autoencoding framework. The basic idea of VADD can also be transferred to discrete diffusion models with other noise schedules (e.g., uniform distribution as the noise), which is an interesting future direction.

#### 3.1 Denoising model in VADD

Instead of parametrizing the backward transition  $p_{\theta}(x_s|x_t)$  as an explicit distribution, we define it as a latent variable model:

$$p_{\theta}(x_s|x_t) = \int_{\mathbb{R}^d} p_{\theta}(x_s|x_t, z) p(z) dz, \quad (6)$$

where  $p(z)$  is the prior distribution of the latent variable  $z \in \mathbb{R}^d$  and  $p_{\theta}(x_s|x_t, z)$ , an explicit probabilistic model, is the conditional distribution given the previous state  $x_t$  and the latent variable  $z$ . Although the conditional distribution  $p_{\theta}(x_s|x_t, z)$  may not capture the dimensional correlations of  $x_s$ , the marginal transition distribution  $p_{\theta}(x_s|x_t)$  is capable of doing this by integrating out  $z$ . Throughout this paper, the prior distribution  $p(z)$  is the standard Gaussian distribution  $\mathcal{N}(\mathbf{0}_d, \mathbf{I}_d)$ , and other multimodal distributions, e.g., Gaussian mixtures, are meaningful to explore in the future.

Inspired by the  $x_0$ -prediction parameterization of MDM backward transitions in equation (2), we parametrize the conditional distribution as  $p_{\theta}(x_s|x_t, z) = \prod_{i=1}^N p_{\theta}(x_s^i|x_t^i, z)$  and

$$p_{\theta}(x_s^i|x_t^i, z) = \begin{cases} \text{Cat}(x_s^i; x_t^i), & x_t^i \neq [\text{M}]; \\ \text{Cat}\left(x_s^i; \frac{1-\alpha_s}{1-\alpha_t} \delta_{[\text{M}]} + \frac{\alpha_s - \alpha_t}{1-\alpha_t} \mu_{\theta}^i(x_t, z, t)\right), & x_t^i = [\text{M}]; \end{cases} \quad (7)$$

where the  $\mu_{\theta}(x_t, z, t) \in \mathbb{R}^{N \times (V+1)}$ , satisfying  $\sum_{j=1}^V \mu_{\theta}^{i,j}(x_t, z, t) = 1$  and  $\mu_{\theta}^{i,[\text{M}]}(x_t, z, t) = 0$ , is a deep model outputting the categorical probabilities of  $p_{\theta}(x_0|x_t, z)$ .

Intuitively, there are multiple possible ways to recover the clean data  $x_0$  from the partially masked sample  $x_t$ , reflecting the multimodality of  $q(x_0|x_t)$ . The latent variable  $z$  can be interpreted as a controller for high-level semantics, guiding the denoising model toward a specific mode of the clean data. Figure 1 provides a comprehensive example on how VADD works on 2D toy examples.

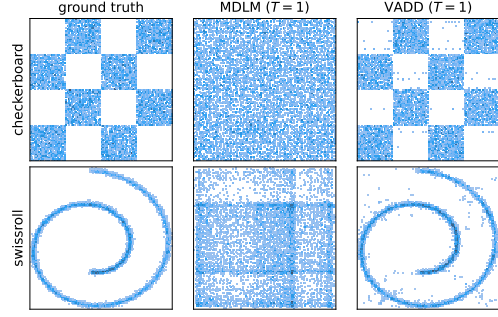


Figure 1: One-step samples of VADD and MDLM (Sahoo et al., 2024) on 2D examples.

---

**Algorithm 1:** Training in VADD

---

**Input:** Number of iterations  $H$ ; Optimizer Opt; KL annealing weight  $\lambda_h$ ; Batch size  $B$ .

Initialize  $p_{\theta}(\mathbf{x}_0|\mathbf{x}_t, \mathbf{z})$  and  $r_{\phi}(\mathbf{z}|\mathbf{x}_0, \mathbf{x}_t)$ ;

**for**  $h = 1, \dots, H$  **do**

    Sample  $\{\mathbf{x}_0^{(b)}\}_{b=1}^B$  from the training data and  $\{t^{(b)}\}_{b=1}^B$  from Uniform(0, 1);

    Sample  $\{\mathbf{x}_{t^{(b)}}^{(b)}\}_{b=1}^B$  based on  $\{\mathbf{x}_0^{(b)}\}_{b=1}^B$  and the forward masking process  $q(\mathbf{x}_t|\mathbf{x}_0)$ ;

    Sample  $\{\mathbf{z}^{(b)}\}_{b=1}^B$  from the recognition model  $r_{\phi}(\mathbf{z}|\mathbf{x}_0^{(b)}, \mathbf{x}_{t^{(b)}}^{(b)})$ ;

    Compute the KL annealing weight  $\lambda_h$ ;

    Compute the Monte Carlo estimate of DELBO  $\widehat{\mathcal{L}}_{\lambda_h, \text{MC}}(\boldsymbol{\theta}, \boldsymbol{\phi}) := \frac{1}{B} \sum_{b=1}^B \widehat{\mathcal{L}}_{\lambda_h}(\mathbf{x}_0^{(b)}; \boldsymbol{\theta}, \boldsymbol{\phi})$ ;

    Update the parameters  $\boldsymbol{\theta}, \boldsymbol{\phi} \leftarrow \text{Opt}(\boldsymbol{\theta}, \boldsymbol{\phi}, -\nabla_{\boldsymbol{\theta}, \boldsymbol{\phi}} \widehat{\mathcal{L}}_{\lambda_h, \text{MC}}(\boldsymbol{\theta}, \boldsymbol{\phi}))$ ;

---

We see that MDLM cannot model this correlation in one step, as suggested by the collapsed samples in the middle column. In contrast, VADD correctly captures this correlation and generates good samples from these multimodal distributions in one step.

Combining equation (6) and (7), the conditional distribution of  $\mathbf{x}_0$  given  $\mathbf{x}_t$ ,  $q(\mathbf{x}_0|\mathbf{x}_t)$ , is approximated through

$$p_{\theta}(\mathbf{x}_0|\mathbf{x}_t) = \int_{\mathbb{R}^d} \prod_{i=1}^N \left[ \boldsymbol{\mu}_{\theta}^{i, \mathbf{x}_0^i}(\mathbf{x}_t, \mathbf{z}, t) \mathbb{I}_{\mathbf{x}_t^i = [\mathbb{M}]} + \mathbb{I}_{\mathbf{x}_0^i = \mathbf{x}_t^i \neq [\mathbb{M}]} \right] p(\mathbf{z}) d\mathbf{z}. \quad (8)$$

However, directly maximizing the ELBO  $\mathcal{L}(\mathbf{x}_0; \boldsymbol{\theta})$  in equation (3) is no longer feasible, since  $p_{\theta}(\mathbf{x}_0|\mathbf{x}_t)$  in VADD requires marginalizing out  $\mathbf{z}$  which is intractable (equation (8)). In what follows, we introduce an alternative tractable surrogate for the ELBO  $\mathcal{L}(\mathbf{x}_0; \boldsymbol{\theta})$  in equation (3).

### 3.2 The variational autoencoding mechanism

Inspired by the idea of VAEs (Kingma & Welling, 2014), we consider approximating the posterior distribution of the latent variable  $\mathbf{z}$  with an auxiliary recognition model  $r_{\phi}(\mathbf{z}|\mathbf{x}_0, \mathbf{x}_t) \approx p_{\theta}(\mathbf{z}|\mathbf{x}_0, \mathbf{x}_t)$ . Now for the  $\mathcal{L}(\mathbf{x}_0; \boldsymbol{\theta})$  in equation (3), by treating the  $p_{\theta}(\mathbf{x}_0|\mathbf{x}_t)$  itself as a marginal likelihood conditioned on  $\mathbf{x}_t$ , the following equation gives a lower bound of  $\mathcal{L}(\mathbf{x}_0; \boldsymbol{\theta})$ :

$$\widehat{\mathcal{L}}(\mathbf{x}_0; \boldsymbol{\theta}, \boldsymbol{\phi}) = \int_0^1 \mathbb{E}_{q(\mathbf{x}_t|\mathbf{x}_0)} \mathbb{E}_{r_{\phi}(\mathbf{z}|\mathbf{x}_0, \mathbf{x}_t)} \frac{-\alpha'_t}{1 - \alpha_t} \log \left( \frac{p_{\theta}(\mathbf{x}_0|\mathbf{x}_t, \mathbf{z}) p(\mathbf{z})}{r_{\phi}(\mathbf{z}|\mathbf{x}_0, \mathbf{x}_t)} \right) dt \leq \mathcal{L}(\mathbf{x}_0; \boldsymbol{\theta}). \quad (9)$$

The  $\widehat{\mathcal{L}}(\mathbf{x}_0; \boldsymbol{\theta}, \boldsymbol{\phi})$  in equation (9) is referred to as the Double Evidence Lower Bound (DELBO), as it is a lower bound of ELBO (see more details in Appendix A.1). In our implementation, the recognition model  $r_{\phi}(\mathbf{z}|\mathbf{x}_0, \mathbf{x}_t)$  is a diagonal Gaussian distribution, i.e.,

$$r_{\phi}(\mathbf{z}|\mathbf{x}_0, \mathbf{x}_t) = \mathcal{N}(\mathbf{m}_{\phi}(\mathbf{x}_0, \mathbf{x}_t), \text{diag}\{\boldsymbol{\sigma}_{\phi}^2(\mathbf{x}_0, \mathbf{x}_t)\}), \quad (10)$$

where  $\mathbf{m}_{\phi}$  and  $\boldsymbol{\sigma}_{\phi}$  are two deep models approximating the mean and standard deviation, respectively. We find that this simple implementation works fairly well in numerical studies.

Similarly to the classical VAEs, the denoising model and recognition model can be jointly optimized by maximizing the DELBO  $\widehat{\mathcal{L}}(\mathbf{x}_0; \boldsymbol{\theta}, \boldsymbol{\phi})$  for all  $\mathbf{x}_0$  in the training set. Since the  $r_{\phi}(\mathbf{z}|\mathbf{x}_0, \mathbf{x}_t)$  is a Gaussian distribution, the reparameterization trick could be utilized to compute the gradient w.r.t.  $\boldsymbol{\phi}$ . However, as the posterior distribution  $p_{\theta}(\mathbf{z}|\mathbf{x}_0, \mathbf{x}_t)$  is rather complex in the high-dimensional cases, naively maximizing  $\widehat{\mathcal{L}}(\mathbf{x}_0; \boldsymbol{\theta}, \boldsymbol{\phi})$  can encounter with the posterior collapse issue empirically. To tackle this problem, we borrow the idea of KL annealing from Bowman et al. (2015); Yang et al. (2017) and consider the following variant of DELBO

$$\widehat{\mathcal{L}}_{\lambda}(\mathbf{x}_0; \boldsymbol{\theta}, \boldsymbol{\phi}) = \int_0^1 \mathbb{E}_{q(\mathbf{x}_t|\mathbf{x}_0)} \mathbb{E}_{r_{\phi}(\mathbf{z}|\mathbf{x}_0, \mathbf{x}_t)} \frac{-\alpha'_t}{1 - \alpha_t} \left[ \log p_{\theta}(\mathbf{x}_0|\mathbf{x}_t, \mathbf{z}) - \lambda \log \left( \frac{r_{\phi}(\mathbf{z}|\mathbf{x}_0, \mathbf{x}_t)}{p(\mathbf{z})} \right) \right] dt, \quad (11)$$

where  $\lambda \in [0, 1]$  is the KL annealing weight. We summarize the training procedure of VADD in Algorithm 1.

### 3.3 Sampling from VADD

As in other MDMs, sampling from VADD also starts from an all-masked state and recovers the clean data with the backward transition  $p_{\theta}(\mathbf{x}_s|\mathbf{x}_t)$ . More specifically, given a time sequence  $\{t_i\}_{i=1}^T$  satisfying  $0 = t_0 < t_1 < \dots < t_T = 1$ , sampling from  $p_{\theta}(\mathbf{x}_0)$  is realized by recursively sampling

$$\mathbf{z}_{t_i} \sim p(\mathbf{z}) \text{ and } \mathbf{x}_{t_{i-1}} \sim p_{\theta}(\mathbf{x}_{t_{i-1}}|\mathbf{x}_{t_i}, \mathbf{z}_{t_i}),$$

starting from  $\mathbf{x}_{t_T} = [\mathbf{M}]^N$ . We refer to this sampling procedure as the **vanilla sampler**.

Recall that in VADD, the latent variable  $\mathbf{z}$  is interpreted to capture high-level semantics of the data. To preserve a consistent semantic representation throughout the entire reverse process, we propose fixing the latent variable across all denoising steps. This leads to the **consistency sampler** that we refer to as VADD-CS. Specifically, we draw a single latent variable  $\mathbf{z}_{\text{fix}} \sim p(\mathbf{z})$  once at the beginning, along with  $\mathbf{x}_{t_T} = [\mathbf{M}]^N$  which is then progressively denoised by sampling from the  $p_{\theta}(\mathbf{x}_{t_{i-1}}|\mathbf{x}_{t_i}, \mathbf{z}_{\text{fix}})$  for each step  $t_i$ . While the transition kernel  $p_{\theta}(\mathbf{x}_s|\mathbf{x}_t)$  remains unchanged from the vanilla sampler, the marginal distribution over the final output  $\mathbf{x}_0$  is modified due to the fixed latent semantics. We summarize the sampling procedure of VADD in Algorithm 2.

---

#### Algorithm 2: Sampling from VADD

---

**Input:** A sequence of time steps  $0 = t_0 < t_1 < \dots < t_T = 1$ ; A transition model  $p_{\theta}(\mathbf{x}_s|\mathbf{x}_t, \mathbf{z})$ .  
**Output:** The generated sample  $\mathbf{x}_0$ .  
Initialize  $\mathbf{x}_{t_T} = [\mathbf{M}]^N$ ;  
**if** Use consistency sampler **then**  
    Sample  $\mathbf{z}_{\text{fix}} \sim p(\mathbf{z})$ ;  
**for**  $i = T, \dots, 1$  **do**  
    **if** Use consistency sampler **then**  
         $\mathbf{z} = \mathbf{z}_{\text{fix}}$ ;  
    **else**  
        Sample  $\mathbf{z} \sim p(\mathbf{z})$ ;  
    Sample  $\mathbf{x}_{t_{i-1}} \sim p_{\theta}(\mathbf{x}_{t_{i-1}}|\mathbf{x}_{t_i}, \mathbf{z})$ ;

---

### 3.4 Design of the denoising model and recognition model for texts

An important application of VADD is text generative modeling. However, the standard transformer architecture (Vaswani et al., 2017) is not directly applicable for parametrizing the denoising model and recognition model for text generation. In this section, we address this limitation by specifically modifying the transformer architecture for both models and analyzing their inference complexities. Denote by  $L$  the number of transformer blocks, by  $d_e$  the dimension of token embeddings, by  $d_c$  the dimension for latent variable embeddings, and by  $d$  the latent dimension.

**Denoising model** Recall that the the backward transition  $q_{\theta}(\mathbf{x}_s|\mathbf{x}_t)$  is implicitly defined by the denoising model  $\mu_{\theta}(\mathbf{x}_t, \mathbf{z}, t)$  in equation (7), whose workflow is illustrated in Figure 2(a). To incorporate  $\mathbf{z}$ , we introduce the AdaLN layer, an affine transform depending on  $\mathbf{z}$ , that performs adaptive layer normalization (AdaLN) (Xu et al., 2019). Specifically, an inner-block MLP first takes the embedding of  $\mathbf{z}$  as input and outputs the shift and scale that will be applied to all token embeddings in the sequence. Each of the  $L$  transformer blocks consists of a self-attention layer and a feed-forward layer, both preceded by an AdaLN layer.

**Recognition model** The recognition model  $r_{\phi}(\mathbf{z}|\mathbf{x}_0, \mathbf{x}_t)$  takes two sequences,  $\mathbf{x}_0$  and  $\mathbf{x}_t$ , as input, but naively applying a transformer to them will double the computational cost. Fortunately, the observation that  $\mathbf{x}_t$  is a partially masked version of  $\mathbf{x}_0$  inspires a simpler model design. We introduce a binary vector  $\mathbf{M}_t \in \{0, 1\}^N$  representing whether a position is masked ( $= 1$ ) or not ( $= 0$ ), and thus the pair  $(\mathbf{x}_0, \mathbf{x}_t)$  can be bijectively mapped to  $(\mathbf{x}_0, \mathbf{M}_t)$  which is used as model input instead. This defines the recognition model  $r_{\phi}(\mathbf{z}|\mathbf{x}_0, \mathbf{M}_t) = r_{\phi}(\mathbf{z}|\mathbf{x}_0, \mathbf{x}_t)$ , as illustrated in Figure 2(b). Similarly to the denoising model, an AdaLN layer is added before both the self-attention layer and feed-forward layer in each transformer block, with the difference that this AdaLN layer is applied exclusively to masked tokens. This operation can be implemented by first defining a learnable mask representation vector  $\mathbf{R}_{\phi}$  (shared across blocks), then using two inner-block MLPs on  $\mathbf{R}_{\phi}$  for outputting the shift and scale of the AdaLN layers in each block, and finally blocking their application to the unmasked tokens by multiplying  $\mathbf{M}_t$ .

**Remark.** *Although a more straightforward way for building  $r_{\phi}(\mathbf{z}|\mathbf{x}_0, \mathbf{x}_t)$  is just ignoring the dependency on  $\mathbf{x}_t$  and only taking  $\mathbf{x}_0$  as input, we find this will cause severe posterior collapse issue empirically, even if the KL annealing weight in the loss function (11) is carefully tuned by us.*

**Complexity analysis** For VADD, since both  $\mathbf{z}$  and  $\mathbf{R}_{\phi}$  are one-dimensional tensors, the complexity of the AdaLN layers is  $O(LNd_e + Ld_c d_e)$ , where  $N$  is the sequence length. For the denoising

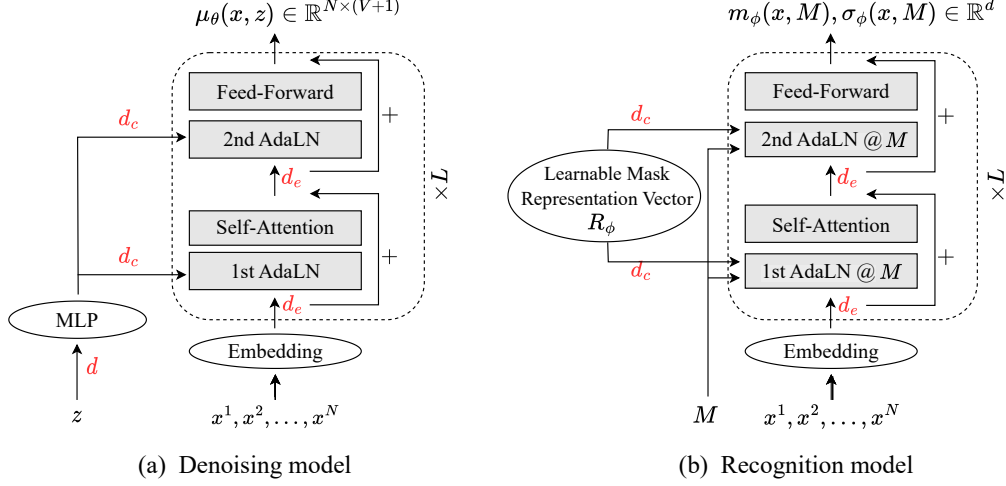


Figure 2: The network architecture of the denoising model and recognition model in VADD for text modeling. The feature dimensions of the tensors are marked in red font.  $@ M$  means that the module is only applied to the positions  $i$  satisfying  $M^i = 1$ .

model, the complexity of MLP is  $O(dd_c)$ , and that of the standard transformer model is  $O(NVd_e + L(N^2d_e + Nd_e^2))$ . Therefore, the total complexity of the denoising model is  $O(NVd_e + L(N^2d_e + Nd_e^2) + LNd_e + Ld_c d_e + dd_c)$ . Since the term  $(Ld_c d_e + dd_c)$  is dominated, the overall complexity is thus to be  $O(VNd_e + L(N^2d_e + Nd_e^2) + LNd_e)$ . For the recognition model, the complexity of the AdaLN layer and transformer model remain the same as in the denoising model, while the complexity of the MLP is  $O(dd_e)$ . Thus, the total complexity of the recognition model is  $O(VNd_e + L(N^2d_e + Nd_e^2) + LNd_e + Ld_c d_e + dd_e) = O(VNd_e + L(N^2d_e + Nd_e^2) + LNd_e)$ . By factorizing  $N$  out, the per-token complexity for both the denoising and recognition model is  $O(Vd_e + LNd_e + Ld_e^2)$ , where we omit the last term as it is one order smaller than the other terms.

It should be pointed out that the training cost of VADD nearly doubles that of other MDMs with only a denoising model, since two models of the same size are jointly trained in VADD using the KL-annealed DELBO loss (11). However, the sampling cost of VADD is the same as that of other MDMs, since the sampling procedure does not involve the recognition model.

## 4 Related works

Several works have explored utilizing latent variable models to improve text modeling (Bowman et al., 2015; Gu et al., 2018; Kaiser et al., 2018). Recently, Kong et al. (2025) used latent variable structure for the next token prediction in autoregressive models and optimized with variational Bayes (Jordan et al., 1999), instead of the VAE amortizing over all training samples. Hayakawa et al. (2024) considered distilling the pretrained MDMs with model mixtures as the backward transition by optimizing the consistency loss. Our approach is clearly distinct from Hayakawa et al. (2024) as we train the latent-variable denoising model from scratch within the framework of VAEs.

## 5 Experiments

In this section, we demonstrate the effectiveness of VADD on three tasks: two-dimensional toy examples, pixel-level image generation, and text generation. For all these tasks, we reimplement MDM using the ELBO loss function defined in equation (3), along with the same training strategy as VADD. This reimplementation serves as our main baseline, which we refer to as MDLM, a method concurrently proposed by three recent works (Sahoo et al., 2024; Shi et al., 2024; Ou et al., 2025). Unless otherwise specified, we use the linear noise schedule  $\alpha_t = 1 - t$  and the linear time steps  $t_i = i/T$  for discretizing the backward process. For the ELBO evaluation in VADD, we use the 1000-sample lower bound variant of DELBO (see equation (20)) as an estimate for ELBO, which is a common choice in the VAE literature (Burda et al., 2016; Vahdat & Kautz, 2020). For all the negative-

Table 1: Empirical JS divergence ( $\downarrow$ ) between generated samples and ground truth samples, and NLL ( $\downarrow$ ) evaluated on ground truth data. JS- $T$  means sampling with  $T$  steps. The empirical JS divergences are evaluated based on 100K samples.

Model	checkerboard			swissroll			circles		
	JS-1	JS-5	NLL	JS-1	JS-5	NLL	JS-1	JS-5	NLL
MDLM	1.395	0.211	8.503	2.619	0.287	7.111	2.273	0.263	7.462
VADD	0.062	<b>0.048</b>	<b>8.058</b>	0.086	<b>0.025</b>	<b>6.132</b>	<b>0.161</b>	<b>0.042</b>	<b>6.716</b>
VADD-CS	<b>0.061</b>	0.049	–	<b>0.085</b>	<b>0.025</b>	–	0.164	0.043	–

likelihood-based metrics, the autoregressive results are exact likelihoods, while the diffusion results are upper bounds. The experimental details can be found in Appendix B. We emphasize that VADD is expected to achieve improved sample-quality-based metrics, such as FID score and generative perplexity, with fewer sampling steps. However, we do not expect substantial improvements in likelihood-based metrics, e.g., bits per dimension, perplexity, etc.

### 5.1 Two-dimensional toy examples

We first apply VADD to two-dimensional toy examples to provide a concise understanding of how our method works. We consider three multimodal distributions: checkerboard, swissroll, and circles. The training set consists of 100K samples generated by the `scikit-learn` package (Pedregosa et al., 2011). We rescale the data to  $[0, 1]$  and discretize them with a bin width of 0.01, resulting in  $V = 100$  for each dimension. Both MDLM and VADD are trained for 500 epochs with a batch size of 256 and an initial learning rate of 3e-4 (annealing according to a cosine schedule). The KL annealing weight  $\lambda$  in VADD linearly increases from 0 to 1 in the first 100 epochs. The latent dimension is set to  $d = 2$ .

Table 1 reports the Jensen-Shannon (JS) divergence and negative marginal loglikelihood (NLL) of different methods, where we see that the VADD outperforms MDLM by a large margin on these quantitative metrics. Interestingly, we do not find a remarkable difference between the vanilla sampler and the consistency sampler, which can be partially attributed to the low data dimension. Figure 1 and Figure 5 show the histplots of the samples generated by different methods and sampling steps, where we see that VADD is capable of generating samples that are much closer to the ground truth.

### 5.2 Pixel-level image generation

We then apply VADD to the pixel-level image generation task on the binarized MNIST (padded to  $32 \times 32$ ,  $V = 2$ ) and CIFAR-10 ( $32 \times 32$ ,  $V = 256$ ) datasets. For both datasets, the denoising model and the recognition model adopt the UNet architecture in the PyTorch implementation<sup>3</sup> of variational diffusion models (Kingma et al., 2021). The denoising model incorporates the latent variable  $z$  by adding its embedding to the pixel embeddings in each up block and down block. The recognition model employs the siamese mechanism (Koch et al., 2015), which applies the same UNet to  $x_0$  and  $x_t$  and finally aggregates the outputs. The denoising model in the MDLM baseline also adopts the same UNet architecture. Both MDLM and VADD are trained for 0.2M (binarized MNIST) or 1M (CIFAR-10) iterations with a batch size of 256 and a constant learning rate of 2e-4. The KL annealing weight  $\lambda$  in VADD linearly increases from 0 to 1 in the first 100K iterations.

Table 2 reports the bits per dimension (BPD) of different models. For the CIFAR-10 results in Table 2, both MDLM and VADD are trained for 2M iterations to keep consistent with that of MD4 (Shi et al., 2024). We see that the latent variable structure provides more generative modeling capacity, as evidenced by the lower BPD of VADD. It is worth noting that the BPD reduction of VADD is much more significant on the binarized MNIST dataset, as the VAE framework generally works better on low-dimensional cases (a smaller  $V$ ).

The binarized MNIST samples generated by MDLM and VADD-CS with different sampling steps are plotted in Figure 3. We see that VADD-CS can generate realistic digit images with even  $T = 5$  sampling steps, which is impossible for MDLM. See more samples in Figure 8, 9 in Appendix C.2. For a direct metric for the sample quality, we report the Fréchet inception distance (FID) score

<sup>3</sup><https://github.com/addtt/variational-diffusion-models>

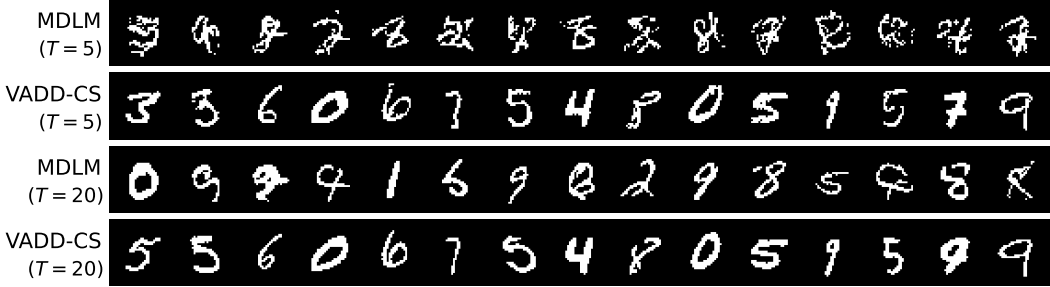


Figure 3: Non-cherry-picked samples generated by different discrete diffusion models and sampling steps on the binarized MNIST dataset.

Table 2: Test BPD ( $\downarrow$ ) on binarized MNIST and CIFAR-10.  $\dagger$ Reproduced by us.

Model	#Parameters	BPD
<i>Binarized MNIST (32 <math>\times</math> 32)</i>		
MDLM $^\dagger$	2.2M	0.075
<b>VADD (ours)</b>	2.3M	<b>0.063</b>
<i>CIFAR-10 (32 <math>\times</math> 32)</i>		
D3PM - $L_{\lambda=0.01}$	37M	4.40
MD4	28M	2.75
MDLM $^\dagger$	32M	2.80
<b>VADD (ours)</b>	32M	<b>2.74</b>

Table 3: FID score ( $\downarrow$ ) with different sampling steps  $T$  on the CIFAR-10 dataset. The FID score is computed with 50K images using the `clean-fid` package.  $\dagger$ Reproduced by us.

$T$	MDLM $^\dagger$	VADD	VADD-CS
10	334.3	170.3	<b>168.6</b>
20	261.3	108.7	<b>104.8</b>
30	203.4	84.8	<b>78.6</b>
40	166.1	72.1	<b>64.8</b>
50	140.3	64.6	<b>56.1</b>
100	76.5	50.5	<b>41.1</b>

between the generated images and the training set on CIFAR-10 in Table 3. We see that VADD consistently generates more realistic images than MDLM with a small number of sampling steps  $T$ , and the consistency sampler performs slightly better. However, it should be acknowledged that the pixel-level discrete modeling of images is quite hard, and the FID scores of MDM-based methods lag behind those of continuous modeling methods by a large margin.

### 5.3 Text generation

Finally, we test the effectiveness of VADD for unconditional text generation, aligned with the common practice of diffusion language models. We consider two widely used datasets: One Billion Word (LM1B) and OpenWebText. The denoising model and recognition model of VADD adopt the architecture in Lou et al. (2024) based on diffusion transformer, with necessary modifications for incorporating the latent variable described in Section 3.4. The reimplemented MDLM baseline also adopts the architecture in Lou et al. (2024). The sizes of these models all correspond to the GPT-2 small scale (around 125M parameters), i.e.,  $T = 12, d_e = 784$ , although our VADD may have slightly more parameters introduced by the AdaLN layers (around 6%). In our implementation, the denoising model and recognition model ignore the dependency on the time  $t$ , following Ou et al. (2025). For both MDLM and VADD, we use the AdamW optimizer with a constant learning rate of 2e-4 (after 2500 warm-up iterations) and an exponential moving average decay rate of 0.9999. The KL annealing weight in VADD increases linearly from 0 to 1 in the first 200K iterations. The results are collected after 1M iterations with a batch size of 512.

**One Billion Word** The One Billion Word (LM1B) (Chelba et al., 2013) is a medium-sized and real-world dataset containing about 30M sentences. Following He et al. (2022); Lou et al. (2024), we use the standard train-test split, tokenize the data with the `bert-base-uncased` tokenizer, and reorganize the data into sequences with a length of  $N = 128$ . The latent dimension in VADD is set to  $d = 128$ . Two additional autoregressive baselines, Transformer-XL (Dai et al., 2019) with 0.8B parameters and OmniNet (Tay et al., 2021) with 0.1B parameters, are considered.

The perplexities on the test split of LM1B are reported in Table 4. Our VADD achieves the best test perplexity among both the autoregressive and diffusion baselines. Note that VADD with only 1M

Table 4: Test perplexities ( $\downarrow$ ) on LM1B. \*Reported in Sahoo et al. (2024).  $\dagger$ Reproduced by us. The other results are reported in their original papers. All shaded model sizes correspond to GPT-2 small.

	Model	#Iterations	Perplexity
AR	Transformer-XL	-	23.5
	OmniNet <sub>T</sub>	-	21.5
	Transformer*	0.5M	22.32
	Transformer*	5M	20.86
Diffusion	DiffusionBert	1.9M	63.78
	SEDD-Absorb	1M	32.79
	MDLM*	1M	27.04
	MDLM*	10M	23.00
	MDLM $\dagger$	1M	27.70
	VADD (ours)	1M	<b>20.53</b>

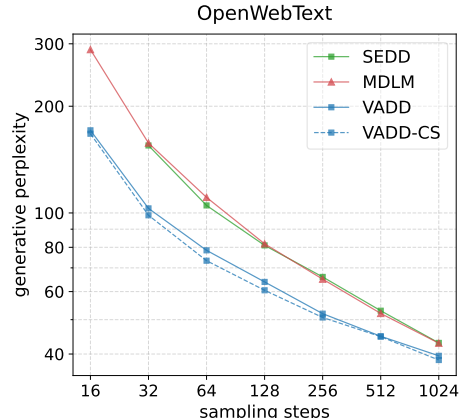


Figure 4: Generative perplexities ( $\downarrow$ ) evaluated by a pre-trained GPT-2 large model based on 256 samples on OpenWebText. All model sizes correspond to GPT-2 small.

Table 5: Zero-shot perplexities ( $\downarrow$ ) on six benchmark datasets of models trained on the OpenWebText. All models are trained for 1M iterations. Results of GPT-2 are reported in Sahoo et al. (2024).  $\dagger$ Reproduced by us. Other results are reported in their original papers.

Test dataset	Lambada	LM1B	WikiText	AG News	PubMed	Arxiv
GPT-2 (Radford et al., 2019)	51.28	51.25	25.75	52.09	49.01	41.73
SEDD-Absorb (Lou et al., 2024)	50.92	79.29	40.62	-	-	-
RADD-AO (Ou et al., 2025)	49.43	70.71	35.25	-	-	-
MDLM $\dagger$ (Sahoo et al., 2024)	49.67	71.03	35.61	68.57	42.43	37.92
<b>VADD (ours)</b>	<b>47.30</b>	<b>69.71</b>	<b>34.78</b>	<b>68.00</b>	<b>40.62</b>	<b>36.39</b>

iterations even surpasses the strongest autoregressive Transformer with 5M iterations. A possible explanation is that the sequences in the reorganized dataset contain around 75% padding tokens that won’t be generated, making VAE especially powerful for this relatively low-dimensional problem.

**OpenWebText** The OpenWebText an open-source replicate of GPT-2’s WebText dataset (Radford et al., 2019). Following Lou et al. (2024), we use the last 100K documents as the test split, tokenize the data with the GPT-2 tokenizer, and reorganize the data into sequences with a length of  $N = 1024$ . The latent dimension in VADD is set to  $d = 512$ . For the zero-shot learning task, we compute the perplexities of the trained model on the test splits of six datasets: Lambada, LM1B, WikiText, AG News, PubMed, and Arxiv, following Sahoo et al. (2024).

According to the generative perplexities with 16~1024 sampling steps depicted in Figure 4, VADD consistently and significantly improves upon other MDM baselines, especially when the number of sampling steps is small. Compared to MDLM, our VADD uses less than 50% computational cost to achieve the same sample quality. The reason lies in VADD’s capability of modeling the joint distribution on multiple tokens. Table 5 reports zero-shot perplexities on six benchmark datasets. In most datasets, our VADD model achieves similar or better zero-shot perplexities than baselines, and we emphasize that MDLM $\dagger$  uses the same architecture and training setting as VADD and is considered as the most appropriate baseline. This observation meets our expectation that VADD has more advantage in the sample-quality-based metrics than the test-likelihood-based metrics.

## 6 Conclusion

In this paper, we present Variational Autoencoding Discrete Diffusion (VADD), which extends the denoising distributions in MDMs with the latent variable structure, allowing for enhanced correlation

modeling over different dimensions. This advantage of VADD makes it possible for correctly generating multiple dimensions simultaneously and is especially powerful with a small number of sampling steps. The variational autoencoding mechanism is utilized to jointly optimize the denoising model together with an auxiliary recognition model. Extensive experiments on image and text generation demonstrate that our VADD consistently outperforms the MDM baselines in terms of sample fidelity. Our approach is the first try of applying latent variable models and variational autoencoding mechanism to MDMs, and other expressive latent variable model designs and efficient optimization methods would be interesting future directions.

## Acknowledgements

This work was supported by National Natural Science Foundation of China (grant no. 12201014, grant no. 12292980 and grant no. 12292983). The research of Cheng Zhang was support in part by National Engineering Laboratory for Big Data Analysis and Applications, the Key Laboratory of Mathematics and Its Applications (LMAM) and the Key Laboratory of Mathematical Economics and Quantitative Finance (LMEQF) of Peking University. The authors appreciate Fangyu Ding and Ding Ding for constructive discussion on this project. The authors are grateful for the computational resources provided by the High-performance Computing Platform of Peking University.

## References

Jacob Austin, Daniel D Johnson, Jonathan Ho, Daniel Tarlow, and Rianne van den Berg. Structured denoising diffusion models in discrete state-spaces. *Advances in Neural Information Processing Systems*, 34:17981–17993, 2021.

A. Blattmann, Robin Rombach, Huan Ling, Tim Dockhorn, Seung Wook Kim, Sanja Fidler, and Karsten Kreis. Align your latents: High-resolution video synthesis with latent diffusion models. *2023 IEEE/CVF Conference on Computer Vision and Pattern Recognition (CVPR)*, pp. 22563–22575, 2023.

Samuel R Bowman, Luke Vilnis, Oriol Vinyals, Andrew M Dai, Rafal Jozefowicz, and Samy Bengio. Generating sentences from a continuous space. *arXiv preprint arXiv:1511.06349*, 2015.

Yuri Burda, Roger B. Grosse, and Ruslan Salakhutdinov. Importance weighted autoencoders. In *International Conference on Learning Representations*, 2016.

Andrew Campbell, Joe Benton, Valentin De Bortoli, Thomas Rainforth, George Deligiannidis, and Arnaud Doucet. A continuous time framework for discrete denoising models. *Advances in Neural Information Processing Systems*, 35:28266–28279, 2022.

Ciprian Chelba, Tomas Mikolov, Mike Schuster, Qi Ge, Thorsten Brants, Philipp Koehn, and Tony Robinson. One billion word benchmark for measuring progress in statistical language modeling. *arXiv preprint arXiv:1312.3005*, 2013.

Zihang Dai, Zhilin Yang, Yiming Yang, Jaime G Carbonell, Quoc Le, and Ruslan Salakhutdinov. Transformer-xl: Attentive language models beyond a fixed-length context. In *Proceedings of the 57th Annual Meeting of the Association for Computational Linguistics*, pp. 2978–2988, 2019.

Jiatao Gu, James Bradbury, Caiming Xiong, Victor OK Li, and Richard Socher. Non-autoregressive neural machine translation. In *International Conference on Learning Representations*, 2018.

Satoshi Hayakawa, Yuhta Takida, Masaaki Imaizumi, Hiromi Wakaki, and Yuki Mitsufuji. Distillation of discrete diffusion through dimensional correlations. In *Workshop on Machine Learning and Compression, NeurIPS 2024*, 2024. URL <https://openreview.net/forum?id=ibx05X7kxc>.

Zhengfu He, Tianxiang Sun, Kuanning Wang, Xuanjing Huang, and Xipeng Qiu. Diffusion-ber: Improving generative masked language models with diffusion models. *arXiv preprint arXiv:2211.15029*, 2022.

Jonathan Ho, Ajay Jain, and Pieter Abbeel. Denoising diffusion probabilistic models. *Advances in Neural Information Processing Systems*, 33:6840–6851, 2020.

Jonathan Ho, Tim Salimans, Alexey A. Gritsenko, William Chan, Mohammad Norouzi, and David J. Fleet. Video diffusion models. In *Advances in Neural Information Processing Systems*, 2022.

Michael I. Jordan, Zoubin Ghahramani, T. Jaakkola, and Lawrence K. Saul. An introduction to variational methods for graphical models. *Machine Learning*, 37:183–233, 1999.

Lukasz Kaiser, Samy Bengio, Aurko Roy, Ashish Vaswani, Niki Parmar, Jakob Uszkoreit, and Noam Shazeer. Fast decoding in sequence models using discrete latent variables. In *International Conference on Machine Learning*, pp. 2390–2399. PMLR, 2018.

D. P. Kingma and M. Welling. Auto-encoding variational bayes. In *ICLR*, 2014.

Diederik Kingma, Tim Salimans, Ben Poole, and Jonathan Ho. Variational diffusion models. *Advances in neural information processing systems*, 34:21696–21707, 2021.

Gregory Koch, Richard Zemel, Ruslan Salakhutdinov, et al. Siamese neural networks for one-shot image recognition. In *ICML deep learning workshop*, volume 2, pp. 1–30. Lille, 2015.

Deqian Kong, Minglu Zhao, Dehong Xu, Bo Pang, Shu Wang, Edouardo Honig, Zhangzhang Si, Chuan Li, Jianwen Xie, Sirui Xie, et al. Scalable language models with posterior inference of latent thought vectors. *arXiv preprint arXiv:2502.01567*, 2025.

Zhifeng Kong, Wei Ping, Jiaji Huang, Kexin Zhao, and Bryan Catanzaro. Diffwave: A versatile diffusion model for audio synthesis. In *International Conference on Learning Representations*, 2021.

Anji Liu, Oliver Broadrick, Mathias Niepert, and Guy Van den Broeck. Discrete copula diffusion. *arXiv preprint arXiv:2410.01949*, 2024.

Haohe Liu, Zehua Chen, Yi Yuan, Xinhao Mei, Xubo Liu, Danilo Mandic, Wenwu Wang, and Mark D Plumley. AudioLDM: Text-to-audio generation with latent diffusion models. In *Proceedings of the 40th International Conference on Machine Learning*, volume 202 of *Proceedings of Machine Learning Research*, pp. 21450–21474, 2023.

Aaron Lou, Chenlin Meng, and Stefano Ermon. Discrete diffusion modeling by estimating the ratios of the data distribution. In *Forty-first International Conference on Machine Learning*, 2024. URL <https://openreview.net/forum?id=CNicRIVIPA>.

Jingyang Ou, Shen Nie, Kaiwen Xue, Fengqi Zhu, Jiacheng Sun, Zhenguo Li, and Chongxuan Li. Your absorbing discrete diffusion secretly models the conditional distributions of clean data. In *The Thirteenth International Conference on Learning Representations*, 2025.

Fabian Pedregosa, Gaël Varoquaux, Alexandre Gramfort, Vincent Michel, Bertrand Thirion, Olivier Grisel, Mathieu Blondel, Peter Prettenhofer, Ron Weiss, Vincent Dubourg, et al. Scikit-learn: Machine learning in python. *the Journal of machine Learning research*, 12:2825–2830, 2011.

Alec Radford, Jeffrey Wu, Rewon Child, David Luan, Dario Amodei, Ilya Sutskever, et al. Language models are unsupervised multitask learners. *OpenAI blog*, 1(8):9, 2019.

Aditya Ramesh, Prafulla Dhariwal, Alex Nichol, Casey Chu, and Mark Chen. Hierarchical text-conditional image generation with clip latents. *ArXiv*, abs/2204.06125, 2022.

Robin Rombach, Andreas Blattmann, Dominik Lorenz, Patrick Esser, and Björn Ommer. High-resolution image synthesis with latent diffusion models, 2021.

Subham Sekhar Sahoo, Marianne Arriola, Aaron Gokaslan, Edgar Mariano Marroquin, Alexander M Rush, Yair Schiff, Justin T Chiu, and Volodymyr Kuleshov. Simple and effective masked diffusion language models. In *The Thirty-eighth Annual Conference on Neural Information Processing Systems*, 2024.

Jiaxin Shi, Kehang Han, Zhe Wang, Arnaud Doucet, and Michalis Titsias. Simplified and generalized masked diffusion for discrete data. *Advances in Neural Information Processing Systems*, 37: 103131–103167, 2024.

Yang Song, Jascha Sohl-Dickstein, Diederik P Kingma, Abhishek Kumar, Stefano Ermon, and Ben Poole. Score-based generative modeling through stochastic differential equations. *arXiv preprint arXiv:2011.13456*, 2020.

Haoran Sun, Lijun Yu, Bo Dai, Dale Schuurmans, and Hanjun Dai. Score-based continuous-time discrete diffusion models. In *The Eleventh International Conference on Learning Representations*, 2023.

Yi Tay, Mostafa Dehghani, Vamsi Aribandi, Jai Gupta, Philip M Pham, Zhen Qin, Dara Bahri, Da-Cheng Juan, and Donald Metzler. Omnidnet: Omnidirectional representations from transformers. In *International Conference on Machine Learning*, pp. 10193–10202. PMLR, 2021.

Arash Vahdat and Jan Kautz. NVAE: A deep hierarchical variational autoencoder. In *Neural Information Processing Systems (NeurIPS)*, 2020.

Ashish Vaswani, Noam Shazeer, Niki Parmar, Jakob Uszkoreit, Llion Jones, Aidan N Gomez, Łukasz Kaiser, and Illia Polosukhin. Attention is all you need. *Advances in neural information processing systems*, 30, 2017.

Jingjing Xu, Xu Sun, Zhiyuan Zhang, Guangxiang Zhao, and Junyang Lin. Understanding and improving layer normalization. *Advances in neural information processing systems*, 32, 2019.

Minkai Xu, Tomas Geffner, Karsten Kreis, Weili Nie, Yilun Xu, Jure Leskovec, Stefano Ermon, and Arash Vahdat. Energy-based diffusion language models for text generation. *arXiv preprint arXiv:2410.21357*, 2024.

Zichao Yang, Zhiting Hu, Ruslan Salakhutdinov, and Taylor Berg-Kirkpatrick. Improved variational autoencoders for text modeling using dilated convolutions. In *International conference on machine learning*, pp. 3881–3890. PMLR, 2017.

Kaiwen Zheng, Yongxin Chen, Hanzi Mao, Ming-Yu Liu, Jun Zhu, and Qinsheng Zhang. Masked diffusion models are secretly time-agnostic masked models and exploit inaccurate categorical sampling. In *The Thirteenth International Conference on Learning Representations*, 2025. URL <https://openreview.net/forum?id=CTC7CmirNr>.

## A Derivations of the DELBO

### A.1 The lower bound of ELBO

Let  $r_\phi(z|x_0, x_t)$  be a recognition model with support on  $\mathbb{R}^d$ , which can simply realized by assuming a Gaussian family for  $r_\phi(z|x_0, x_t)$ . We have

$$\int_{\mathbb{R}^d} \frac{p_\theta(x_0|x_t, z)p(z)}{r_\phi(z|x_0, x_t)} r_\phi(z|x_0, x_t) dz = \int_{\mathbb{R}^d} p_\theta(x_0|x_t, z)p(z) dz = p_\theta(x_0|x_t). \quad (12)$$

Using Jensen's inequality and noting that  $\log()$  is a concave function, we have

$$\log p_\theta(x_0|x_t) = \log \int_{\mathbb{R}^d} \frac{p_\theta(x_0|x_t, z)p(z)}{r_\phi(z|x_0, x_t)} r_\phi(z|x_0, x_t) dz \quad (13)$$

$$\geq \int_{\mathbb{R}^d} \log \left( \frac{p_\theta(x_0|x_t, z)p(z)}{r_\phi(z|x_0, x_t)} \right) r_\phi(z|x_0, x_t) dz \quad (14)$$

$$= \mathbb{E}_{r_\phi(z|x_0, x_t)} \log \left( \frac{p_\theta(x_0|x_t, z)p(z)}{r_\phi(z|x_0, x_t)} \right). \quad (15)$$

The inequality (14) in holds if and only if  $r_\phi(z|x_0, x_t) = p_\theta(z|x_0, x_t)$ . By noting that  $-\frac{\alpha'_t}{1-\alpha_t} > 0$ , we have

$$\hat{\mathcal{L}}(x_0; \theta, \phi) := \int_0^1 \mathbb{E}_{q(x_t|x_0)} \mathbb{E}_{r_\phi(z|x_0, x_t)} \frac{-\alpha'_t}{1-\alpha_t} \log \left( \frac{p_\theta(x_0|x_t, z)p(z)}{r_\phi(z|x_0, x_t)} \right) dt \quad (16)$$

$$\leq \int_0^1 \mathbb{E}_{q(x_t|x_0)} \frac{-\alpha'_t}{1-\alpha_t} \log p_\theta(x_0|x_t) dt \quad (17)$$

$$= \mathcal{L}(x_0; \theta). \quad (18)$$

The inequality (17) holds if and only if for any  $t \in [0, 1]$  and  $x_t \sim q(x_t|x_0)$ , it holds that  $r_\phi(z|x_0, x_t) = p_\theta(z|x_0, x_t)$ .

Finally, we conclude that the following chain of lower bounds:

$$\hat{\mathcal{L}}(x_0; \theta, \phi) \leq \mathcal{L}(x_0; \theta) \leq \log p_\theta(x_0). \quad (19)$$

### A.2 The multi-sample variant of DELBO for estimating ELBO

For previous MDMs, e.g., Sahoo et al. (2024); Shi et al. (2024); Ou et al. (2025), the ELBO  $\mathcal{L}(x_0; \theta)$  is reported as a surrogate of the intractable likelihood  $\log p_\theta(x_0)$  and then used to compute the perplexities, bits per dimension, etc. However, for VADD, computing the ELBO is intractable as the integration on  $z$  is intractable. We consider the following multi-sample variant of the DELBO, termed  $K$ -sample DELBO,

$$\hat{\mathcal{L}}_K(x_0; \theta, \phi) = \int_0^1 \mathbb{E}_{q(x_t|x_0)} \mathbb{E}_{z^1, \dots, z^K \sim r_\phi(z|x_0, x_t)} \frac{-\alpha'_t}{1-\alpha_t} \log \left( \frac{1}{K} \sum_{i=1}^K \frac{p_\theta(x_0|x_t, z^K)p(z^K)}{r_\phi(z^K|x_0, x_t)} \right) dt. \quad (20)$$

The  $K$ -sample DELBO satisfies

$$\hat{\mathcal{L}}_K(x_0; \theta, \phi) \leq \hat{\mathcal{L}}_{K+1}(x_0; \theta, \phi) \leq \mathcal{L}(x_0; \theta). \quad (21)$$

Moreover, by the strong law of large numbers, it holds that

$$\lim_{K \rightarrow \infty} \hat{\mathcal{L}}_K(x_0; \theta, \phi) = \mathcal{L}(x_0; \theta). \quad (22)$$

In all of our experiments, we use  $\hat{\mathcal{L}}_{1000}(x_0; \theta, \phi)$  as an approximation for the  $\mathcal{L}(x_0; \theta)$ . For the Monte Carlo sampling on  $(x_t, t)$ , we sample 100 independent pairs  $(x_t, t) \sim q(x_t|x_0) \cdot U[0, 1]$  to estimate the  $\hat{\mathcal{L}}_{1000}(x_0; \theta, \phi)$ .

### A.3 The likelihood lower bound of the consistency sampler

The consistency sampler fixes a  $\mathbf{z}$  along the backward process, which can be understood as a standard MDM with backward transition distribution  $p_{\theta}(\mathbf{x}_0|\mathbf{x}_t, \mathbf{z})$ . Given a fixed  $\mathbf{z}$ , the conditional ELBO on  $p(\mathbf{x}_0)$  is

$$\mathcal{L}^{\text{CS}}(\mathbf{x}_0; \theta, \mathbf{z}) := \int_0^1 \mathbb{E}_{q(\mathbf{x}_t|\mathbf{x}_0)} \frac{-\alpha'_t}{1-\alpha_t} \log p_{\theta}(\mathbf{x}_0|\mathbf{x}_t, \mathbf{z}) dt. \quad (23)$$

Integrating out  $\mathbf{z}$  will give the ELBO on  $p(\mathbf{x}_0)$  as

$$\mathcal{L}^{\text{CS}}(\mathbf{x}_0; \theta) := \int_{\mathbb{R}^d} \mathcal{L}^{\text{CS}}(\mathbf{x}_0; \theta, \mathbf{z}) p(\mathbf{z}) d\mathbf{z} = \int_0^1 \mathbb{E}_{q(\mathbf{x}_t|\mathbf{x}_0)} \mathbb{E}_{p(\mathbf{z})} \frac{-\alpha'_t}{1-\alpha_t} \log p_{\theta}(\mathbf{x}_0|\mathbf{x}_t, \mathbf{z}) dt. \quad (24)$$

We compare  $\mathcal{L}^{\text{CS}}(\mathbf{x}_0; \theta)$  with  $\mathcal{L}(\mathbf{x}_0; \theta)$  and  $\hat{\mathcal{L}}(\mathbf{x}_0; \theta, \phi)$ , formalized as Proposition 1 and Proposition 2, respectively.

**Proposition 1.** *For all  $\mathbf{x}_0$ , it holds that  $\mathcal{L}^{\text{CS}}(\mathbf{x}_0; \theta) \leq \mathcal{L}(\mathbf{x}_0; \theta)$ .*

*Proof.* The difference between the integrand functions in equation (3) and equation (24) is

$$\log p_{\theta}(\mathbf{x}_0|\mathbf{x}_t) - \mathbb{E}_{p(\mathbf{z})} \log p_{\theta}(\mathbf{x}_0|\mathbf{x}_t, \mathbf{z}) \quad (25)$$

$$= \log \left( \int_{\mathbb{R}^d} \log p_{\theta}(\mathbf{x}_0|\mathbf{x}_t, \mathbf{z}) p(\mathbf{z}) d\mathbf{z} \right) - \int_{\mathbb{R}^d} p(\mathbf{z}) \log p_{\theta}(\mathbf{x}_0|\mathbf{x}_t, \mathbf{z}) d\mathbf{z} \quad (26)$$

$$\geq 0 \quad (27)$$

where the inequality is because of Jensen's inequality. Taking expectation of equation (25) w.r.t.  $\mathbf{x}_t$  and  $t$  gives

$$\mathcal{L}(\mathbf{x}_0; \theta) - \mathcal{L}^{\text{CS}}(\mathbf{x}_0; \theta) \geq 0. \quad (28)$$

□

**Proposition 2.** *Denote the cross entropy between two distributions  $p(\mathbf{x})$  and  $q(\mathbf{x})$  by  $H(p, q) = -\int p(\mathbf{x}) \log q(\mathbf{x}) d\mathbf{x}$ . Assume  $H(r_{\phi}(\mathbf{z}|\mathbf{x}_0, \mathbf{x}_t), p_{\theta}(\mathbf{z}|\mathbf{x}_0, \mathbf{x}_t)) \geq H(p(\mathbf{z}), p_{\theta}(\mathbf{z}|\mathbf{x}_0, \mathbf{x}_t))$  and  $H(p(\mathbf{z}), p(\mathbf{z})) \geq H(r_{\phi}(\mathbf{z}|\mathbf{x}_0, \mathbf{x}_t), p(\mathbf{z}))$ , i.e.,  $r_{\phi}(\mathbf{z}|\mathbf{x}_0, \mathbf{x}_t)$  is a better approximation of  $p_{\theta}(\mathbf{z}|\mathbf{x}_0, \mathbf{x}_t)$  than  $p(\mathbf{z})$ . Then we have  $\mathcal{L}^{\text{CS}}(\mathbf{x}_0; \theta) \geq \hat{\mathcal{L}}(\mathbf{x}_0; \theta, \phi)$ .*

*Proof.* The difference between the integrand functions in equation (24) and equation (9) is

$$\mathbb{E}_{p(\mathbf{z})} \log p_{\theta}(\mathbf{x}_0|\mathbf{x}_t, \mathbf{z}) - \mathbb{E}_{r_{\phi}(\mathbf{z}|\mathbf{x}_0, \mathbf{x}_t)} \log \left( \frac{p_{\theta}(\mathbf{x}_0|\mathbf{x}_t, \mathbf{z}) p(\mathbf{z})}{r_{\phi}(\mathbf{z}|\mathbf{x}_0, \mathbf{x}_t)} \right) \quad (29)$$

$$= \int_{\mathbb{R}^d} [p(\mathbf{z}) - r_{\phi}(\mathbf{z}|\mathbf{x}_0, \mathbf{x}_t)] \log p_{\theta}(\mathbf{x}_0|\mathbf{x}_t, \mathbf{z}) d\mathbf{z} - \int_{\mathbb{R}^d} r_{\phi}(\mathbf{z}|\mathbf{x}_0, \mathbf{x}_t) \log \left( \frac{p(\mathbf{z})}{r_{\phi}(\mathbf{z}|\mathbf{x}_0, \mathbf{x}_t)} \right) d\mathbf{z}. \quad (30)$$

For the first term, we have

$$\int_{\mathbb{R}^d} [p(\mathbf{z}) - r_{\phi}(\mathbf{z}|\mathbf{x}_0, \mathbf{x}_t)] \log p_{\theta}(\mathbf{x}_0|\mathbf{x}_t, \mathbf{z}) d\mathbf{z} \quad (31)$$

$$= \int_{\mathbb{R}^d} [p(\mathbf{z}) - r_{\phi}(\mathbf{z}|\mathbf{x}_0, \mathbf{x}_t)] \log p_{\theta}(\mathbf{z}|\mathbf{x}_0, \mathbf{x}_t) d\mathbf{z} + \int_{\mathbb{R}^d} [p(\mathbf{z}) - r_{\phi}(\mathbf{z}|\mathbf{x}_0, \mathbf{x}_t)] \log p_{\theta}(\mathbf{x}_0, \mathbf{x}_t) d\mathbf{z} \quad (32)$$

$$\begin{aligned} & - \int_{\mathbb{R}^d} [p(\mathbf{z}) - r_{\phi}(\mathbf{z}|\mathbf{x}_0, \mathbf{x}_t)] \log p(\mathbf{z}) d\mathbf{z} \\ & = [H(r_{\phi}(\mathbf{z}|\mathbf{x}_0, \mathbf{x}_t), p_{\theta}(\mathbf{z}|\mathbf{x}_0, \mathbf{x}_t)) - H(p(\mathbf{z}), p_{\theta}(\mathbf{z}|\mathbf{x}_0, \mathbf{x}_t))] + 0 \\ & \quad + [H(p(\mathbf{z}), p(\mathbf{z})) - H(r_{\phi}(\mathbf{z}|\mathbf{x}_0, \mathbf{x}_t), p(\mathbf{z}))] \end{aligned} \quad (33)$$

By the assumption on cross entropies, both nonzero terms in equation (33) are equal to or greater than 0. Therefore, we have

$$\int_{\mathbb{R}^d} [p(\mathbf{z}) - r_{\phi}(\mathbf{z}|\mathbf{x}_0, \mathbf{x}_t)] \log p_{\theta}(\mathbf{x}_0|\mathbf{x}_t, \mathbf{z}) d\mathbf{z} \geq 0. \quad (34)$$

For the second term, we have

$$-\int_{\mathbb{R}^d} r_\phi(\mathbf{z}|\mathbf{x}_0, \mathbf{x}_t) \log \left( \frac{p(\mathbf{z})}{r_\phi(\mathbf{z}|\mathbf{x}_0, \mathbf{x}_t)} \right) d\mathbf{z} = \text{KL}(r_\phi(\mathbf{z}|\mathbf{x}_0, \mathbf{x}_t) || p(\mathbf{z})) \geq 0. \quad (35)$$

Therefore, by taking expectation of equation (31) w.r.t.  $\mathbf{x}_t$  and  $t$ , we conclude

$$\mathcal{L}^{\text{CS}}(\mathbf{x}_0; \boldsymbol{\theta}) - \hat{\mathcal{L}}(\mathbf{x}_0; \boldsymbol{\theta}, \boldsymbol{\phi}) \geq 0. \quad (36)$$

□

## B Details of experimental setup

### B.1 Two-dimensional toy examples

We consider three multimodal distributions: checkerboard, swissroll, and circles. The training set consists of 100K samples generated by the `scikit-learn` package (Pedregosa et al., 2011). For checkerboard, `nrows`=2 and `ncols`=2; for the swissroll, `noise`=0.2; for the circles, `noise`=0.02 and `factor`=0.5. We rescale the data to  $[0, 1]$  and discretize them with a bin width of 0.01, resulting in  $V = 100$  for each dimension. The latent dimension is set to  $d = 2$ .

The denoising model  $\mu_\theta(\mathbf{x}_t, \mathbf{z}, t)$  takes a integer-valued sample  $\mathbf{x}_t$ , and a vecotr  $\mathbf{z}$ , and a scalar  $t$  as inputs. All the activation functions in MLPs are ELU unless other specified.  $\mu_\theta(\mathbf{x}_t, \mathbf{z}, t)$  consists of the following two steps:

- **Embedding.** The embedding of  $t$ ,  $\text{emb}(t)$ , is the output of positional sinusoidal embedding (Vaswani et al., 2017) and a following MLP with channel widths [1024, 512, 512]. The embedding of  $\mathbf{z}$ ,  $\text{emb}(\mathbf{z})$ , is the output of an MLP with channel widths [ $d$ , 512]. The embedding of  $\mathbf{x}$ ,  $\text{emb}(\mathbf{x})$ , is the output of an embedding module with embedding dimension 512.
- **Readout.** We then sum up  $\text{emb}(t)$ ,  $\text{emb}(\mathbf{z})$ ,  $\text{emb}(\mathbf{x})$  and apply an MLP with channel width [512, 512, 512, 512, 512,  $V$ ].

The recognition model  $r_\phi(\mathbf{z}|\mathbf{x}_0, \mathbf{x}_t)$  takes two integer-valued vectors  $\mathbf{x}_0, \mathbf{x}_t$  and a scalar value  $t$  as input and output the vector-valued mean and standard deviation of  $\mathbf{z}$ . We consider a Siamese scheme to incorporate the two inputs  $\mathbf{x}_0, \mathbf{x}_t$ .

- **Embedding.** The embedding of  $t$ ,  $\text{emb}(t)$ , is the output of positional sinusoidal embedding (Vaswani et al., 2017) and a following MLP with channel widths [1024, 512, 512]. The embeddings of  $\mathbf{x}_0$  and  $\mathbf{x}_t$ ,  $\text{emb}(\mathbf{x}_0)$  and  $\text{emb}(\mathbf{x}_t)$ , are the output of the same embedding module with embedding dimension 512.
- **Readout.** We then apply MLP with channel width [512, 512, 512, 512, 512, 512] on  $\text{emb}(t) + \text{emb}(\mathbf{x}_0)$  and  $\text{emb}(t) + \text{emb}(\mathbf{x}_t)$ , and obtain the outputs  $\text{out}_0$  and  $\text{out}_t$ . Finally, we compute the average of  $\text{out}_0$  and  $\text{out}_t$ , and apply an MLP with channel width [512, 512, 2 $d$ ].

We use the Adam optimizer with momentum parameters  $(\beta_1, \beta_2) = (0.9, 0.999)$  and weight decay 0. The initial learning rate is 3e-4 and decreases according to a cosine annealing schedule. The KL annealing weight increases linearly from 0 to 1 in the first 100 epochs. The batch size is 256. The total number of training epochs is 500. The experiments are run on a single A100 40G GPU.

### B.2 Pixel-level image generation

The binarized MNIST data binarized MNIST ( $32 \times 32, V = 2$ ) are obtained by binarizing the grayscale MNIST data with a threshold of 0.5 and padding 2 zeros on each side of the image. CIFAR-10 ( $32 \times 32, V = 256$ ) can be directly obtained in its original form without any transformation.

The denoising model and the recognition model adopt the UNet architecture in the PyTorch implementation (<https://github.com/adattt/variational-diffusion-models>) of variational diffusion models (Kingma et al., 2021).

- **Binarized MNIST.** For both the recognition model and the denoising model, the numbers of up blocks and down blocks are 8. The embedding dimension is 64. The pixel embedding

dimension is 32. The dropout rate is 0.1. The number of normalization groups is 16. The number of attention heads is 1. The latent dimension is 64.

- **CIFAR-10.** For both the recognition model and the denoising model, the numbers of up blocks and down blocks are 32. The embedding dimension is 128. The pixel embedding dimension is 32. The dropout rate is 0.1. The number of normalization groups is 32. The number of attention heads is 32. The latent dimension is 128.

We make the following modifications for the denoising model and the recognition model.

- **Denoising model.** A special token  $[M]$  is also added to the table of the pixel embedding module. We transform the latent variable  $z$  into an embedding  $\text{emb}(z)$  with MLPs and add it to the embeddings of all pixels in each up block and down block.
- **Recognition model.** Borrowing the idea of the siamese mechanism, a standard UNet takes  $(x_0, t)$  and  $(x_t, t)$  as inputs, and outputs two tensors  $\text{out}_0$  and  $\text{out}_t$ . We compute the average  $(\text{out}_0 + \text{out}_t)/2$  and downsample it to a  $1 \times 1 \times 2d$  tensor with down convolution blocks. This  $1 \times 1 \times 2d$  tensor will give the mean and standard deviation of  $r_\phi(z|x_0, x_t)$ .

We use the AdamW optimizer with  $(\beta_1, \beta_2) = (0.9, 0.99)$ , a weight decay of 0.01, and a constant learning rate of 2e-4. The batch size is 256. The gradient is clipped to a maximum norm of 1. The KL annealing weight linearly increases from 0 to 1 in the first 100K iterations. The total number of iterations is 200K for binarized MNIST and 1M for CIFAR-10. The exponential moving average decay rate is 0.9999, and the update frequency is 1. The experiments of binarized MNIST are run on a single A100 40G GPU. The experiments of CIFAR-10 are run on 8 A100 40G GPUs.

### B.3 Text generation

For the One Billion Word dataset, we firstly detokenize the texts following Lou et al. (2024). We then tokenize the texts with the `bert-base-uncased` tokenizer, following He et al. (2022); Lou et al. (2024). We pad and truncate the sequences to a length of 128.

For the OpenWebText dataset, we firstly detokenize the text following Lou et al. (2024). We then tokenize the texts with the GPT-2 tokenizer. We concatenate and wrap them to a sequence length of 1024, including a BOS and a EOS token as the first and last token of the sequence. We use the last 100K documents as the validation split.

The network architecture and inference complexity of the denoising model and the recognition model have been elucidated in Section 3.4. The model size corresponds to the GPT-2 small scale, i.e., 12 transformer blocks, an embedding dimension of 768, and 12 heads in each attention layer.

The optimizer is AdamW with  $(\beta_1, \beta_2) = (0.9, 0.999)$ , a weight decay of 0.0. The learning rate is a constant 3e-4, with a warmup phase of 2500 steps. The batch size is 512. The gradient is clipped to a maximum norm of 1. The KL annealing weight linearly increases from 0 to 1 in the first 100K iterations. The total number of iterations is 1M. The exponential moving average decay rate is 0.9999, and the update frequency is 1. The experiments on One Billion Word are run on 8 A100 40G GPUs, and the experiments on OpenWebText are run on 8 H800 GPUs.

We detokenize the One Billion Words dataset following Lou et al. [33], whose code can be found here<sup>4</sup>. We tokenize the One Billion Words dataset with the `bert-base-uncased` tokenizer, following He et al. [26]. We pad and truncate sequences to a length of 128

## C Additional experimental results

### C.1 Two-dimensional toy examples

Figure 5 shows the histplots of the samples generated by MDLM and VADD. We see that VADD generates samples that are more close to the ground truth with both 1 and 5 sampling steps. We also visualize the samples under 1, 5, 10, 20 sampling steps of VADD and VADD-CS in Figure 6 and Figure 7, respectively. We see that VADD and VADD-CS produce very similar samples in this 2D toy experiment.

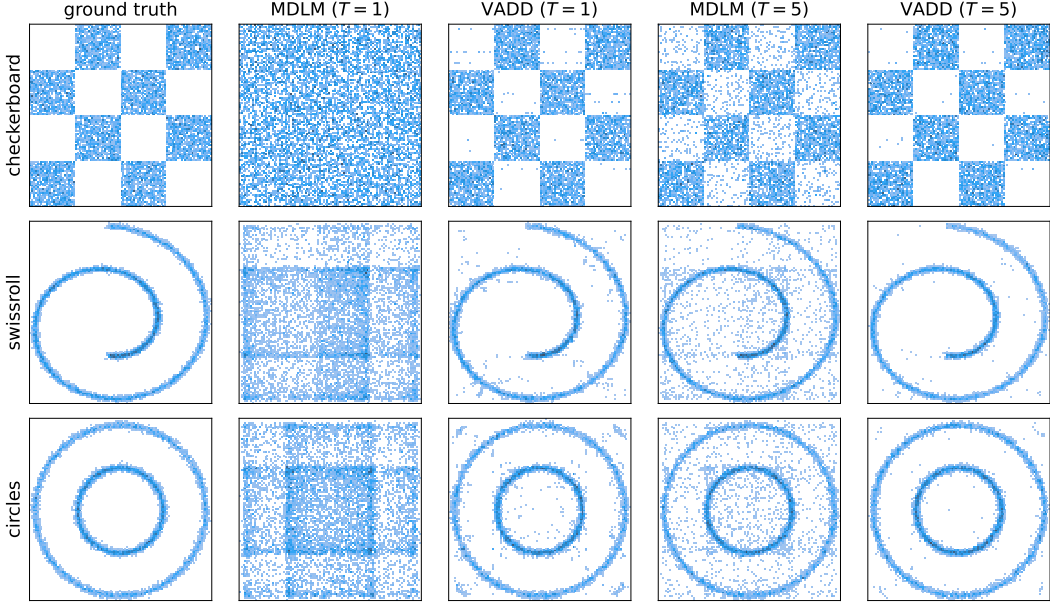


Figure 5: Histplots of the ground truth and the samples generated from different models and sampling steps on the 2D toy example.

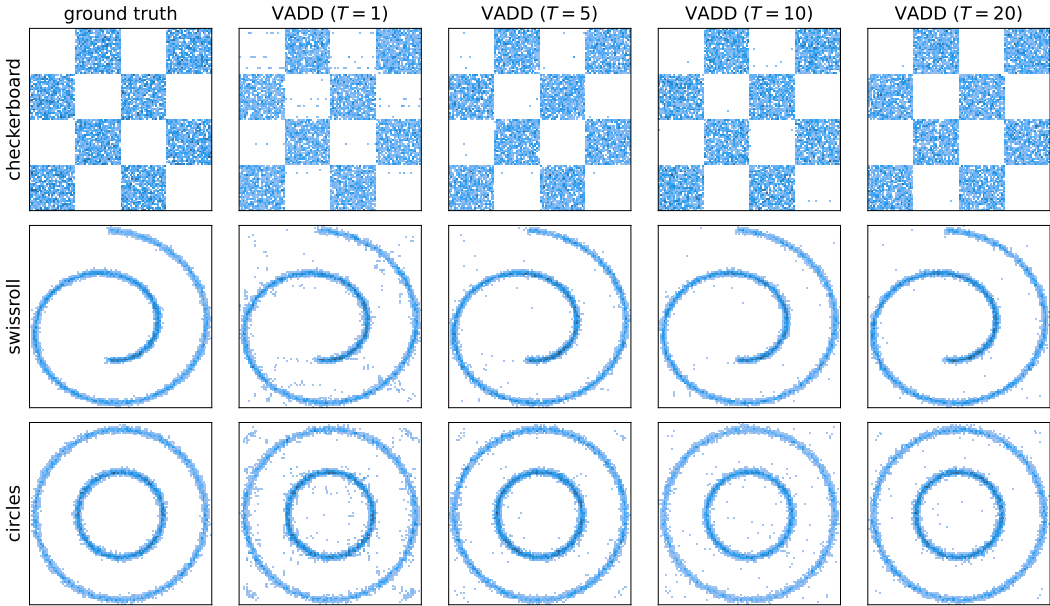


Figure 6: Histplots of the ground truth and the samples generated from VADD with various sampling steps on the 2D toy example.

## C.2 Pixel-level image generation

Figure 8 and Figure 9 provide the binarized samples generated by VADD and VADD-CS, respectively. We see that both VADD and VADD-CS can generate acceptable samples with  $T = 1$  sampling steps. The samples generated by VADD-CS are slightly better than those from VADD.

The training and test negative DELBO curves for VADD and MDLM is plotted in . We see that for both models, the training loss decreases steadily, and VADD will outperform MDLM in the end.

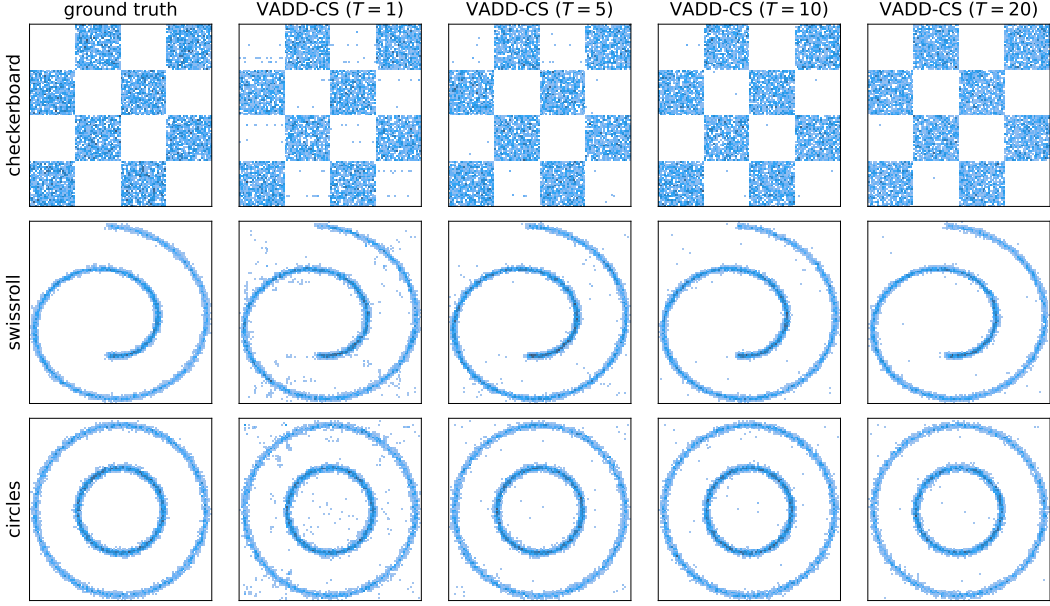


Figure 7: Histplots of the ground truth and the samples generated from VADD-CS with various sampling steps on the 2D toy example.



Figure 8: Samples generated by VADD with different sampling steps on the binarized MNIST.

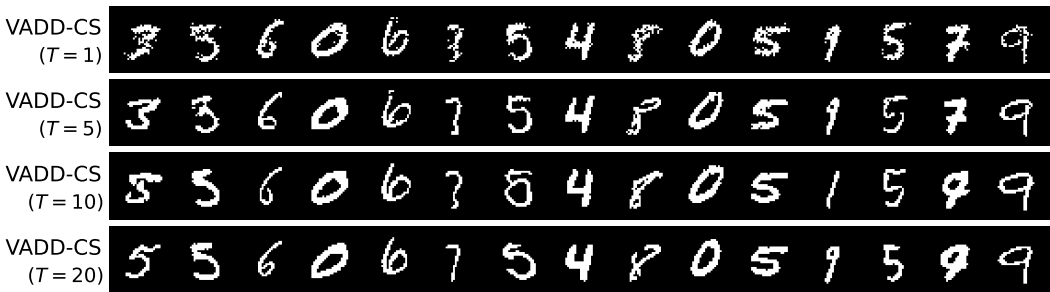


Figure 9: Samples generated by VADD-CS with different sampling steps on the binarized MNIST.

### C.3 Text generation

Table 6 shows the test perplexities on the OpenWebText dataset. To inspect how the number of particles will affect the estimate of ELBO, we also perform an ablation study on the number of particles  $K$  (see the  $K$ -sample DELBO (20)). Note that this estimate is identical to DELBO when  $K = 1$ . We see that the ELBO estimate gradually improves as  $K$  increases.

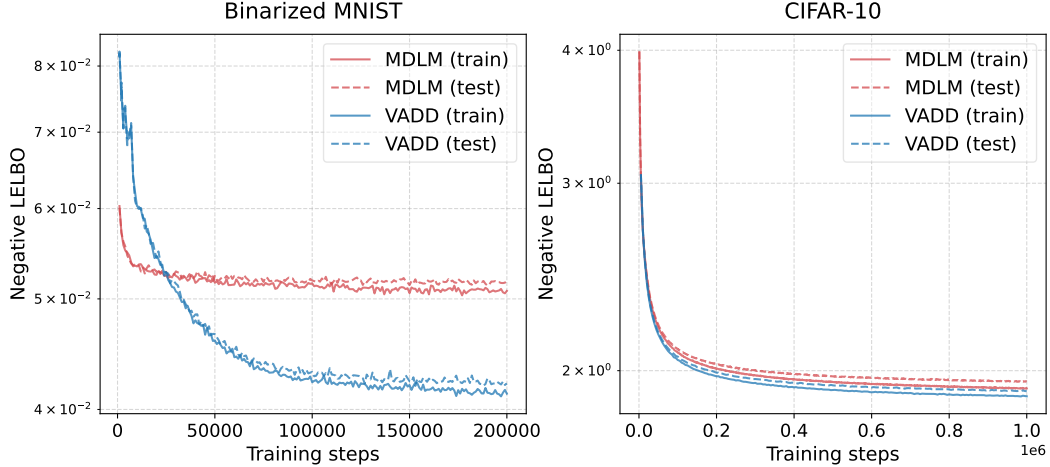


Figure 10: Training and test negative DELBOs on the pixel-level image generation task.

Zheng et al. (2025) points out that the generative perplexity might be sensitive to the precision of categorical sampling. To this end, we compute the generative perplexity using fp64 in Table 7, where we see that VADD consistently outperforms MDLM.

The generated samples from VADD-CS trained on OpenWebText with 128, 256, 512, and 1024 sampling steps are shown in Figure 11-14, respectively. The categorical sampling is under fp32 precision.

Table 6: Perplexities on the test split of OpenWebText. All the models are trained for 1M iterations with a batch size of 512 and a context size of 1024. All model sizes correspond to GPT-2 small.

Model	Perplexity
AR (reproduced by Sahoo et al. (2024))	17.54
SEDD (reproduced by Sahoo et al. (2024))	24.10
MDLM (reported by Sahoo et al. (2024))	23.21
MDLM (reproduced by us)	23.07
VADD ( $K = 1$ )	22.56
VADD ( $K = 10$ )	22.33
VADD ( $K = 50$ )	22.36
VADD ( $K = 100$ )	22.27
VADD ( $K = 1000$ )	<b>22.21</b>

## D Broader impact

This paper presents work whose goal is to advance the field of machine learning. There are many potential societal consequences of our work, none of which we feel must be specifically highlighted here.

Table 7: Generative perplexity of the model trained on OpenWebText. The results are averaged over 256 independent samples. The categorical sampling is done under fp64 precision.

Number of sampling steps ( $T$ )	16	32	64	128	256	512	1024
MDLM (reproduced by us)	330.39	191.96	141.23	124.12	115.12	108.87	104.58
VADD	194.08	124.23	98.82	89.24	85.93	82.11	78.27
VADD-CS	<b>187.67</b>	<b>114.11</b>	<b>93.05</b>	<b>81.68</b>	<b>77.00</b>	<b>75.28</b>	<b>73.96</b>

<|lendoftext|> American culture.

One of the distinguishing marks of experiences that culture tells in a shorter or longer life is that it is committed to telling them in a way that objectively perceives all of them. There is even a competing model of understanding that virtue, but there will always be a number of different ways to express it, a number of more subtle lacking in this respect.<|lendoftext|>First, business can be changing all over the place. We advance for the draft, the preseason, and most then again, even on minor updates. While all the variations are going in a similar direction, there are still some making things more difficult. Teams realize that this isn't the ultimate act of leadership. Fans have been too flound when it comes to garnering fan support for too much time. They use that getting and covering both fans and their teams, in a given year. Fan service can be frustratingly the same, actual quiet life, IPM to watch. So their own management doesn't understand the nuances of changing. they take place without anyone's expectation.

Your worst fear is that owners, not going to understand current market dynamics, might be prone to their refusals to change. The problem with this is that its much safer assuming our best practices. Teams to continually alter their parameters, regardless of their organization, how you ratings are used, or, language will be replaced and wage demand will decrease.

Do owners need to move on, if they change their model, and they plan to change it? Teams will sit down and stay focused. It's simply their business to compete. This case with growth without growth and innovative strategy. For leagues with high turnover and payroll, it is unsustainable.

Three years ago, it was third in revenue with its base of 400 million. For the 40 years this particular league is living, the turnover rates will fully continue to grow. This is the "social economics" of video game regulation. At best, there's a semi-permanent equilibrium in play.

In other words, even if owner knows they're playing around with a draft, or all known work contracts, it will take a while for some meaningful change to evolve. There is an unwillingness to find a way to assess the value of playing money in the kitty differently.

Who does not want to be on the team because they should be? The stark contrast of how the overall marketplace operates shows just how uncomfortable finding ways to change it can be.

The things I enjoy watching in football is that learning new concepts is a good thing, when they are trying to create an experiences or two. But leagues have too many to find it attractive.

Modern ideas and institutions arise out of necessity. More information, more mechanical units who have time to be available everywhere. In order to succeed more successfully, you have to build infrastructure.

If you have the championship you, then have janetents and coaches who train on the gridiron. As revenues get worse year after year, and you people will throw away talent and hope that life will change, because you must have a model who is already enfeuded into the league or other traditional sports, as opposed to the NFL.

What has been between league and practice over the past decade, which is now where they've been from innovators, is a clear indication that this sport needs to be something to take seriously. This seismic shift in growth and turn of events, and then the shift in itself in the form of changes has also been brutal. I a look toward the future in Formula 1. In a dominant race, you tend to regress to constant levels, and Roger Penske losing his performance-goal regulations means an erosion of market revenues. In the lisp, has morals, will likely move on.

A good cross-section of growth rate of a couple sports leagues also shows clear disruptive trends, and the mid-tier leagues report they found that they're left behind because of participation. Even with attendance levels growing.

So it is also true that a coach is not unlikely to gains any recognition for their boosters much than a parent would get similar benefits to him. Or, it means that they are the bottom end, behind that team will even be more in a position in respect to revenues that they put up.

Players on one side of the equation should know that pay commissions cut. But let's be a lecher. These simple payments aren't the priority for players, paid well. For players, a bad statement. Franchise players on that side, franchises are critical. And if companies want, you put their corporate-based clubs to the table.

On the other side, if they want an easy ride inside the league and you let it to them by any investors somewhere in the world, one is certainly going to be able to convince any owner to do the rest of their business in order to conform to reality.<|lendoftext|>

Figure 11: Text sample generated by VADD-CS trained on OpenWebText with 128 sampling steps.

<|lendoftext|> to help us all mature out, so we bring out gifts of good experiences for all by learning and having individual goals everyday, so that I can help them grow. Through some other means, that was my thinking process, about how this game could make both of my kids be the people I want them to be.

And the fact that having each of my daughters capable of is making me selfless, letting me be athletic as well, and have social connection, which is success and private achievement. So, I'm teaching them—we're doing so diverse young adults today but young kids today in this sport—which are what myself believe to be a good performance about the developmental process. Definitely and partially my telling of these stories benefits me from storytelling about the things we can do as a kid and make them happy, and help make me be a good person and how I can be a positive reminder that they're not me.

And one I want to mention, a lot of guys respect the scores. Boys? They respect? I'm against them too, and as more men care about the scores, a lot of my daughters do care about who I am after they're gone and they're WNBA players. And the life and benefits of high school's where it's really meaningful to do something about the level of education level for women. That's a good point to everything we will talk about.

But for guys and for kids, feeling empowered and anxious is fundamentally what all fathers want to do in making making more commitment universally important, and about changing the conversation about how to interact with kids. That was one example of innovation to making conversations about sports easy; it would take a bigger forward, and when we did it, like the OOn, our regional and transformative actions in social impact were small; being hit with negative stereotypes, calling for more men to be masculine, in ways that many of us didn't; and all of these things were well grounded. But also, the fact that we have the sorts of emotional challenges that are very evident in the opportunity to grow the NBA. And of course, besides overall it got a lot improved in areas where both men and women got equal opportunities about teamwork and other than education.

That thing is that I'm proud to be the leader behind the economic growth in this league, because in sports, the education of the growth in sports can be incredibly important, and I'm happy to announce our efforts and my mom's leadership as to what can be done together that can serve our organization about where we stand as a whole.

Now, because of economic development that can motivate people, because of the fact there are more women coaches like me at Oregon, which will have a more positive regional impact on coaches who are more capable, because it really brings a battle-tested sport. And boys are better coaches when it comes to say the least than are women and girls, about coaches among them coming from teams with youth programs, which as well as education, is as important as female players being able to are can impact new young players in their teams and in their basketball and in their sports.

This is a lot of what's important for us; this isn't a time when men are are the male-agers. Where we are and how things are progressing on the ground are significant and those coaches and students who have advocated for the young boys and young girls aren't much better off where teens were in the years before. Those who need help and aren't like single moms who have their lives back without government aid. There are academics who have a study that shows multiple student loans have been rates of success during first grade nationally, which is a lesson and key understanding in how they continue even now.

There is economic growth that's most essential about the economic opportunities that children are being able to access their democratic capital and state — the economic and social opportunities for productivity and development to them. It's also about those rates of access to education and education inequity. Those are really the beginning of a vision I have said we have to have more leadership in these kinds of efforts standing up for young people and democratizing the growth of the adult economies I want to see as well.

That's the part where we wrote about great young athletes, players that everyone knows are used just to show the world. Going with the NBA I, we also look at kids. We teach young players — once for the first time — what kids are supposed to show the world. We figure out how young players in the league can win a post-season title and how they can win a World Championship title. We figure out how they do, and at colleges and universities, we'll find out out which of these kids is going to earn the grades being athletic and which are ultimately going to earn<|lendoftext|>

Figure 12: Text sample generated by VADD-CS trained on OpenWebText with 256 sampling steps.

<|endoftext|> get an average 11th grade. I used to be able to do pretty much anything I grew up doing in high school, so I feel like I would study and do that month work so that, afterward, I developed some of my emotional psychology. And it was really fun, and that's how I came out of school, whether it was through piano or reading or gifted education, it was teaching good to have with the job with me every day. Everything was really organized, I feel like I learned. If I could not make mistakes and keep my family with integrity, as well as me not get my hair out of it, not kind of read and things I needed not knowing but I should have been able to do if I could, then I would learn again that I had reached adulthood. And if I thought I could get there, I would emphasize a part of my youth and make it even better.

I graduated from Wellesley, and I met Steve. There, Steve, he studied our sport, who then transferred to doing science. He went on to meet me, and I think that he understood that drinking, drinking was not something I liked to do as a kid and that I could refine my emotional approach. So, again, we were on the same page, so, across all political identities, we are thousands of years older than our founding generation. I like that, that works very effectively to me. And it made me happy to learn how deaf people like Jimmy Kimmel could make extraordinary political choices to achieve their hopes.

It may be that covering up Donald Trump's successes in the context of his own campaigns was unfortunate, but the whole truth remains that Trump is no less legitimate political character than Hillary Clinton. He's a more than capable candidate right now.

But there are many ways a candidate can change the outcome for citizens. Is there some in order that Trump is in order to make a good campaign get off the ground?

Both the media and the candidates are invested in the campaign making the election make sense — yes, that is the point of more a campaign. While one can say confidently that people will do very well in the forthcoming election, and obviously we aren't entirely persuaded that a candidate in office necessarily means that we will attain the outcome we want, there comes an order to vote on a candidate who is sufficient and have those voters give the chance to reflect on their views with a consistency that are well worth the price for office.

Political parties are determined by a base that built on the other side of that base. To the point of our leader who believes there will be stakes for work over the candidate, one that is winning the election so well, the problem is that a supply of quality requires a significant stake, even to those who vote too any level for a Liberal Party member but who will probably find that a stake is someone who need no stake, but want to interact a building to what first and rank. I know it may not sound to someone in a party with many members, but in this instance that is not a position we deserve to win voters — we have to win voters on some level.

But this seems to be missing at my feelings about winning since I am a former candidate. Instead of a running a and finding votes between parties, I tend a think that immigration is a security issue means that people are supporting immigration as it stands now while the social costs are growing. I think that by winning all the votes provided by a person other than as myself does not get who it really needs to win in the first place. Voting for them is about going to party members who expect to win the election itself. Peering in the background, I still seem to want to feel about the state of the land. Currently, they give candidates away or try to make a break with their candidate paying candidates. For example, the Federalist says it's unlikely that garnering 90

The bad part of this is that if there is any concern or a single issue that voters care about, most people aren't going to evaluate it. They probably are going to accept someone that cares about how affect the outcome. And that preference will be different if a different situation is run in more or less becomes easy. Given how difficult running a campaign is, it's hard to for a vote what policy is best, as we have we fully determined in the under the historical period that we are through, our age always, that we be able to govern in the democratic markets.

It's kind of like trying to lose whites with the groups we know us for very long. When a campaign for a different result to its predecessor allows it to dem the group out of doing the job, then disregarding those people by calling them irrelevant to making any decisions about how we are voting.

What people have to say — what to say to consider, consider<|endoftext|>

Figure 13: Text sample generated by VADD-CS trained on OpenWebText with 512 sampling steps.

<lendoftext>There's a time in my life where I'm going to have to decide two years ago where to go next. The last months have been more competitive than usual sports, getting huge victories and depressing losses. But, on which side of the pitch has to happen in the current market environment? A lot of people will want to jump in and watch the 5 big game, all without having to say goodbye to various friends and extended families. A lot of people will want to enjoy the amount of NBA fun, which is the reason many think ticket prices are going to go up drastically in the future.

It's understandable for the elite sport that when tickets go up millions and millions, that's just good business. What's worse, and often, is not.

In sports, a lot more time is gone for the "socialized" game than it was for football. Players in their 20s are again playing in a lot of small print. This is the case of giving young players growing up the social aspects we understand by buying tickets.

With the coming age of smartphones, and consumers shopping for modern devices and video games, we're going to have to degrade the cultural medium of basketball to the last possible.

There's more sports fans living longer, more often than ever before because of the recession. Though the recession hasn't been around since 2001, the following years are evident the success of that many markets and this country—a microcosm of America. Although it is the absolute fact that sports is sport, it remains by far the only major sport that understands this type of audience, if not shared goals. However, if you look at attendance and new stands, and not ticket sales:(.) and you see that the ticket sales and payroll figures for professional sports are similarly lower across both leagues and the markets. For example, Forbes Business Sports' recent report on this subject also shown that on such a big haul, Indians expect big sales of tickets at every major game of their many teams to raise for the construction of new and better franchises.

The one gate run involved in pro sports reduces the chances of tomorrow's game for a great new team to work. They occur, if the cash flow is already high, which isn't going to make that sustainable team moving forward. The only compelling reason for a good team is upkeep of the fledgling franchises. When it comes time to justify the week (of) the season, brings me to the good part.

Both capital and cost control strictly exceed the spending. The owner has to use how quickly he can to create capital. With Coaches who've made the interview headlines over the last decade for finding a solid balance between the, those playing football and the marketing due to a chance to take, this looks like an upward trajectory. All along, this idea has been a case of "club," team.

In baseball, the league allows you to play at the same level, it's free of a flexible schedule, and is under the marketing budget, opening up to signing up some real talented top players of the best. Once upon a time when a kid is still playing, they're very often told by new head coach Rick Carlisle, "This is why you play your college football."

In my opinion, that's the one I've told for ages that always let me play for NBA teams when I line back up, and say "I care". Sometimes they also realize that I'm in no bad shape.

I know how paid I was to be an NBA player I am not. How much can I enjoy my life outside the NBA, when I don't have to make that happen in the business world. My 3/4 wife and I could probably make more marketing opportunities as a professional, if I put in the majority of my time in college and other places where I know I have a good relationship with my team and I like what I'm doing. And anyway, when it comes to helping new teams, starting players choose between are the very tough choices, but you're trying to make them accept. One part of your job is the lack of the money.

The same, and sending them out that their job is to fill in places their players don't need to fill on the way out, and figure out the intricacies of how to play. But merely recruiting for a truly good player, they've got to be better, and let the talent fall behind.

In the late months of the every year, it's critically important to coach players to get a chance to work your way back into the regular season. But sometimes the road ahead is too long, of small to mass changes.

While a minority of the<lendoftext>

Figure 14: Text sample generated by VADD-CS trained on OpenWebText with 1024 sampling steps.